Fermi National Accelerator Laboratory

FN-443
SSC-N-276
0302.000

Fields, Impedances and Structures*

K.-Y. Ng
Fermi National Accelerator Laboratory
P.O. Box 500, Batavia, Illinois 60510

April 1987

*To be published as a section in *Principles of the High Energy Hadron Colliders, Part I: The SSC,* edited by A.W. Chao and M. Month.

Operated by Universities Research Association Inc. under contract with the United States Department of Energy

FN-443
0302.000
(SSC-N-276)

(Draft December, 1986)
(Final April, 1987)

FIELDS, IMPEDANCES AND STRUCTURES*

King-Yuen Ng

Fermi National Accelerator Laboratory†, *Batavia, IL 60510*

CONTENTS

*To be published as a section in *Principles of the High Energy Hadron Colliders, Part I: The SSC*, edited by A. W. Chao and M. Month.
†Operated by the Universities Research Association, Inc., under contract with the U. S. Department of Energy.

I INTRODUCTION

Beam particles interact directly with the beam particles themselves or indirectly through the electromagnetic fields reflected back from the walls of the vacuum chamber. The interaction between the fields and a bunch may lead to coherent motions of the particles inside the bunch resulting in instabilities. In the frequency domain, we say that the beam current sees longitudinal and transverse impedances due to space charge and the discontinuities of the vacuum chamber.

For the SSC, the bunch intensity is very low because we want to limit the event rate at collision. So the single bunch instabilities encountered in bunched beam storage rings may not be an important issue here. However, in order to reach a designated luminosity, there is an enormous number of bunches. The electromagnetic fields inside the vacuum chamber can couple bunches together and let them oscillate coherently leading to multi-bunch instabilities. A real impedance will cause parasitic beam energy loss. This will heat up the vacuum chamber, some of which occurs at liquid helium temperature and thus contributes to the cryogenic load. The space-charge impedance will lead to a tune shift in single-particle betatron motion, which can increase the transverse beam size and even lead to instability.

For other machines such as an electron storage ring, the rate of interaction decreases sharply with energy. To maintain a certain event rate, we would like to have a particle beam with as high an intensity as possible and as small emittances as possible. Although there are techniques to attain high intensity and low emittances, they are often limited by single bunch instabilities. As a result, these impedances must be kept sufficiently low in order that a beam of high luminosity can be possible.

In this section, we shall firstly discuss the electromagnetic fields left by a particle after traversing some structures of the vacuum chamber. Coupling impedances are next defined in terms of the wake fields. They are then estimated for various discontinuities in the chamber.

II WAKE FIELDS AND IMPEDANCES

First of all, let us take up the problem of a charged particle interacting with a smooth circular vacuum chamber of radius b. The particle has a charge e travelling with a velocity v in the direction of the axis of the beam pipe but at a distance a away from it. In cylindrical coordinate (r, θ, z), the charge density is

$$\rho(r, \theta, z, t) = \frac{e}{a}\delta(r - a)\delta_p(\theta)\delta(z - vt), \tag{2.1}$$

where $\delta_p(\theta)$ denotes the periodic delta function. Through the continuity equation, the current density is

$$J_z(r,\theta,z,t) = \rho(r,\theta,z,t)v. \tag{2.2}$$

Equation (2.1) can be expanded in multipoles:

$$\rho(r,\theta,z,t) = \sum_{m=0}^{\infty} \rho_m, \tag{2.3}$$

where

$$\rho_m = \frac{i_m}{\pi a^{m+1}(1+\delta_{m0})}\delta(r-a)\delta(z-vt)\cos m\theta, \tag{2.4}$$

and $i_m = ea^m$ is the m-th multipole. Similar expansion can be done for the current density;

$$J_z(r,\theta,z,t) = \sum_{m=0}^{\infty} J_{zm}, \tag{2.5}$$

with

$$J_{zm} = \rho_m v. \tag{2.6}$$

The electric field $\mathbf{E}$ and the magnetic field $\mathbf{B}$ can be represented by the potentials V and $\mathbf{A}$,

$$\mathbf{E} = -\nabla V - \dot{\mathbf{A}}, \tag{2.7}$$

$$\mathbf{B} = \nabla \times \mathbf{A}. \tag{2.8}$$

In the Lorentz gauge $\nabla \cdot \mathbf{A} + \dot{V}/c^2 = 0$, c being the velocity of light, the Maxwell's equations can be written as

$$\nabla^2 V - \frac{1}{c^2}\ddot{V} = -\frac{\rho}{\epsilon_0},$$

$$\nabla^2 \mathbf{A} - \frac{1}{c^2}\ddot{\mathbf{A}} = -\mu_0 \mathbf{J}, \tag{2.9}$$

where ϵ_0 and μ_0 are respectively the electric permittivity and magnetic permeability of free space.

Let us first assume that the walls of the beam pipe are infinitely conducting. Since the current density of the particle has only a z component and the beam pipe is smooth, the wall current is also in the z-direction only. From Eq. (2.9), the vector potential $\mathbf{A}$ has therefore only a z-component. As a result, the equations for V and A_z are proportional to each other. In fact,

$$A_z = \mu_0 \epsilon_0 v V. \tag{2.10}$$

Therefore, we need only to solve the equation for V.

We are going to Fourier transform z and t; i. e.,

$$\tilde{\rho}(r,\theta,k_z,w) = \frac{1}{4\pi^2}\int dzdt\rho(r,\theta,z,t)e^{j(k_z z-\omega t)}, \tag{2.11}$$

or taking only the m-th multipole,

$$\tilde{\rho}_m = \frac{i_m}{2\pi^2 a^{m+1}}\delta(r-a)\delta(\omega-k_z v)\cos m\theta. \tag{2.12}$$

The Maxwell's equation for $\tilde{V}$ then reads

$$\frac{1}{r}\frac{\partial}{\partial r}\left(r\frac{\partial\tilde{V}}{\partial r}\right) - \left(k_z^2 - \frac{\omega^2}{c^2} + \frac{m^2}{r^2}\right)\tilde{V} = \frac{\tilde{\rho}_m}{\epsilon_0}. \tag{2.13}$$

The solution is

$$\tilde{V} = \begin{cases} \mathcal{A} I_m(qr)\cos m\theta & \text{if } r < a, \\ \mathcal{B} R_m(qr)\cos m\theta & \text{if } r > a, \end{cases} \tag{2.14}$$

where

$$q^2 = k_z^2 - \frac{\omega^2}{c^2} = k_z^2(1-\beta^2) = \frac{k_z^2}{\gamma^2}, \tag{2.15}$$

$$R_m(qr) = K_m(qr) - I_m(qr)\frac{K_m(qb)}{I_m(qb)}, \tag{2.16}$$

and I_m and K_m are modified Bessel functions of order m of the first and second kind. Note that, by choosing the combination in R_m, we have ensured that V and A_z and therefore E_z vanishes at the walls of the beam pipe. At the boundary $r = a$,

$$\tilde{E}_z = jk_z\tilde{V} - j\omega\tilde{A}_z = \frac{jk_z}{\gamma^2}\tilde{V} \tag{2.17}$$

is continuous, while

$$\tilde{E}_r = -\frac{\partial\tilde{V}}{\partial r} \tag{2.18}$$

has a jump,

$$\tilde{E}_r\,|_{a+} - \tilde{E}_r\,|_{a-} = \int\frac{\tilde{\rho}_m}{\epsilon_0}dr = \frac{i_m\delta(\omega-k_z v)}{4\pi^2\epsilon_0 a^{m+1}}. \tag{2.19}$$

Then, $\mathcal{A}$ and $\mathcal{B}$ can be determined:

$$\mathcal{A} = \frac{i_m\delta(\omega-k_z v)R_m(qa)}{4\pi^2\epsilon_0 q a^{m+1}D_m}, \tag{2.20}$$

$$B = \frac{i_m \delta(\omega - k_z v) I_m(qa)}{4\pi^2 \epsilon_0 q a^{m+1} D_m}, \tag{2.21}$$

where

$$D_m = I'_m(qa) K_m(qa) - I_m(qa) K'_m(qa). \tag{2.22}$$

Now we are in the the position to study the electromagnetic fields generated by the particle. First, let us concentrate on the monopole component or $m = 0$. The source is just a ring of charge e of radius a; so the solution is θ independent. For $r < a$, the longitudinal electric field is, after taking an inverse Fourier transform,

$$E_z(r, z, t) = \int dk_z \frac{j k_z e R_0(qa) I_0(qr)}{4\pi^2 \epsilon_0 \gamma^2 q a D_0} e^{-j k_z (z - vt)}. \tag{2.23}$$

For a charged particle travelling at $z = v(t - \tau)$ or trailing the ring source by $z_0 = v\tau$, the longitudinal electric field per unit source charge seen is given by

$$-W_{0\|}(r, \tau) = \int dk_z \frac{j k_z R_0(qa) I_0(qr)}{4\pi^2 \epsilon_0 \gamma^2 q a D_0} e^{j k_z v \tau}. \tag{2.24}$$

This is the wake field left by the source and is a function of r and τ or z_0 only. The negative sign in front of $W_{0\|}$ is put in on purpose and, as we will see later, this will lead to simple relation to the transverse wake field. For $r > a$, we only need to replace $R_0(qa) I_0(qr)$ in Eq. (2.24) by $I_0(qa) R_0(qr)$. Similar expressions can be written down for E_r and B_θ. When $qb = k_z b/\gamma \ll 1$, the Bessel functions can be expanded and Eq. (2.24) becomes

$$W_{0\|}(r, z_0) = -\int dk_z \frac{j k_z}{4\pi^2 \epsilon_0 \gamma^2} \ln \frac{b}{a} e^{j k_z z_0}, \tag{2.25}$$

or

$$W_{0\|}(r, z_0) = -\frac{\ln(b/a)}{2\pi \epsilon_0 \gamma^2} \delta'(z_0). \tag{2.26}$$

Note that because of the restriction $k_z b/\gamma \ll 1$ has been made, the delta function in Eq. (2.26) should be regarded to have a spread of $z_0 \sim b/\gamma$ or $\tau \sim b/v\gamma$. In fact, this is the spread of the electromagnetic field around the ring source longitudinally. The electric field configuration is plotted in Fig. 1.

Now let us consider a current

$$I(z, t) = I_0 e^{j(\omega t - kz)} \tag{2.27}$$

of cross sectional radius a. The wave velocity v is related to the wave number k by $v = \omega/k$. The charge at position z and time t is affected by those in front of it. The longitudinal electric field seen is

$$E_z(z, t) = -\int dz_0 I_0 e^{j\omega(t - \frac{z + z_0}{v})} \frac{W_{0\|}(z_0)}{v}, \tag{2.28}$$

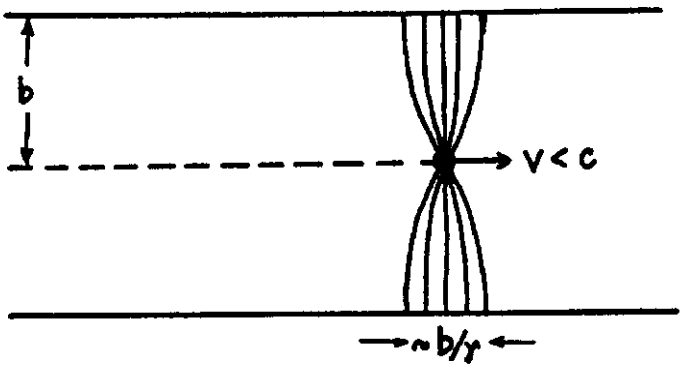

Figure 1: The electric wake field of a particle with velocity v.

or

$$E_z(z,t) = -I(z,t)\int dz_0 \frac{W_{0\|}(z_0)}{v} e^{-j\omega\frac{z_0}{v}}, \tag{2.29}$$

the wake field being evaluated at $r = 0$. We can therefore define a coupling longitudinal impedance $Z_{0\|}(\omega)$ as the drop in potential per unit current over a distance ℓ of the beam pipe, or

$$\frac{Z_{0\|}(\omega)}{\ell} = \int d\tau W_{0\|}(\tau) e^{-j\omega\tau}, \tag{2.30}$$

which is just the Fourier transform of the wake field. Substituting Eq. (2.26) into Eq. (2.30), we obtain for $\omega \ll \gamma v/b$,

$$\frac{Z_{0\|}(\omega)}{\ell} = -\frac{j\omega}{2\pi\epsilon_0\gamma^2 v^2}\ln\frac{b}{a}. \tag{2.31}$$

We see from Eq. (2.27) that v is in fact the phase velocity of the wave. For a storage ring of radius R, we must have $k_z = n/R$, where n is a harmonic number, an integer, denoting the number of wavelengths inside the storage ring. Through a dispersion relation, it can be shown that the frequency of the wave $\omega \sim n\omega_0$. In other words, the wave velocity does not differ very much from the particle velocity. So it will not result in much error if we consider the velocity parameters v, β and γ to be the particle velocity parameters. Introducing the impedance of free space $Z_0 = 1/c\epsilon_0 \sim 377$ ohms, we have, from Eq. (2.31), for the whole ring,

$$\frac{Z_{0\|}(\omega)}{n} = -j\frac{Z_0}{\gamma^2\beta}\ln\frac{b}{a}. \tag{2.32}$$

This is the space-charge impedance for a thin cylindrical current that is hollow inside because the impedance is derived from the wake field of a ring source. For

a non-empty cylindrical beam, we need to start with a source that is a thin disc of radius a and solve the Maxwell's equations again for the wake field. The solution is simple and similar. This leads to the space-charge impedance per unit harmonic of

$$\frac{Z_{0\parallel}(\omega)}{n} = -j\frac{Z_0 g_0}{2\gamma^2\beta}, \tag{2.33}$$

where the geometrical factor g_0 is given by

$$g_0 = 2\ln\frac{b}{a} + 1. \tag{2.34}$$

The extra term besides the logarithmic comes from the field contribution inside the beam.

This space-charge effect is only important when the wave velocity is small. For example, in low energy boosters, it will inevitably lead to microwave growth after transition crossing and therefore the blowup of the bunch area. This is why the low energy booster of the SSC is carefully designed so that the transition gamma is $\gamma_t = 10.5$ while the beam is extracted at 8 GeV/c. Thus, transition crossing is avoided. For an ultra-relativistic wave or $\gamma \to \infty$, we can see from Fig. 1 that the space-charge fields become infinitely thin so that the wake field approaches zero and therefore will not affect any particles behind it. The impedance of Eq. (2.33) also reflects the same result.

If the walls of the beam pipe are not perfectly conducting, E_z will not vanish there. Thus, the solution of $\tilde{V}$, Eq. (2.14), needs alteration for the region $r > a$. This has been worked out in detail in Ref. [1] and will not be repeated here. However, we shall derive it in a different way below (see Section IV). The monopole wake field due to a resistive beam pipe is shown in Fig. 2. The total longitudinal impedance is then

$$\frac{Z_{0\parallel}(\omega)}{n} = -j\frac{Z_0 g_0}{2\gamma^2\beta} + (1+j)\frac{R}{\sigma\delta bn}, \tag{2.35}$$

where σ is the conductivity of the walls of the beam pipe, $\delta = (2/\omega\mu\sigma)^{1/2}$ the skin depth, and the formula holds when $n \ll R\gamma/b$.

The monopole wake field, being cylindrically symmetric, can only modify the longitudinal density of a particle beam. For deflecting forces, we need to go to higher multipoles.

Let us consider the dipole force with $m = 1$. The source consists of a ring of radius a with a $\cos\theta$ charge distribution. For the sake of convenience, let us denote $\theta = 0$ to be the x-direction. Since the source is a pure dipole in the x-direction, we expect the wake field generated would invoke a deflecting force in the x-direction

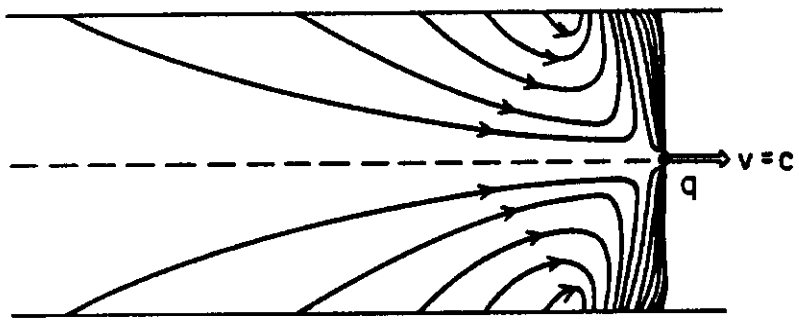

Figure 2: The electric wake field due to the resistivity of the chamber walls.

also. Therefore, we want to compute E_r and B_θ at $\theta = 0$. From Eqs. (2.10), (2.14), (2.18), (2.20) and (2.21), we get

$$\tilde{E}_r = -\frac{i_1 \delta(\omega - k_z v) R_1(qa) I_1'(qr) \cos\theta}{2\pi^2 \epsilon_0 a^2 D_1}, \tag{2.36}$$

$$\tilde{B}_\theta = \frac{v}{c^2} \tilde{E}_r. \tag{2.37}$$

The deflecting force per unit charge is

$$\tilde{F}_\perp = \tilde{E}_r + (\boldsymbol{v} \times \tilde{\mathbf{B}})_r = \frac{\tilde{E}_r}{\gamma^2}, \tag{2.38}$$

or, taking the inverse Fourier transform,

$$F_\perp = -\int d\omega dk_z \frac{i_1 \delta(\omega - k_z v) R_1(qa) I_1'(qr) \cos\theta}{2\pi^2 \epsilon_0 a^2 \gamma^2 D_1} e^{j(\omega t - k_z z)}. \tag{2.39}$$

A dipole charge ring i_1 travelling at $z = v(t - \tau)$ or trailing the source by $z_0 = v\tau$ will see a force splitting the dipole further apart. This force per unit dipole is

$$W_{1\perp}(r, \theta, \tau) = -\int dk_z \frac{R_1(qa) I_1'(qr) \cos\theta}{2\pi^2 \epsilon_0 a^2 \gamma^2 D_1} e^{jk_z v\tau}, \tag{2.40}$$

and is called the dipole transverse wake field. Besides r and θ, it is a function of τ or z_0 only. When $qb = k_z b/\gamma \ll 1$, the Bessel functions can be expanded. Thus,

$$W_{1\perp}(r, \theta, z_0) = -\int dk_z \frac{1}{4\pi^2 \epsilon_0 \gamma^2} \left(\frac{1}{a^2} - \frac{1}{b^2}\right) e^{jk_z z_0}, \tag{2.41}$$

or

$$W_{1\perp}(r,\theta,z_0) = -\frac{1}{2\pi\epsilon_0\gamma^2}\left(\frac{1}{a^2}-\frac{1}{b^2}\right)\delta(z_0). \tag{2.42}$$

Again, because of the restriction $k_x b/\gamma \ll 1$ has been made in the expansion of the Bessel functions, the delta function in Eq. (2.42) and, therefore, the transverse wake field should be regarded to have a spread of $z_0 \sim b/\gamma$ or $\tau \sim b/v\gamma$.

For a dipole current

$$I_1(z,t) = I_{10}e^{j(\omega t - kz)}, \tag{2.43}$$

where $I_{10} \propto \cos\theta$ and the wave velocity $v = \omega/k$. The transverse force per unit charge seen by a dipole element at position z and time t is given by

$$F_\perp(z,t) = \int dz_0 I_{10} e^{j\omega(t-\frac{z+z_0}{v})}\frac{W_{1\perp}(r,z_0)}{v}, \tag{2.44}$$

where the transverse wake field is evaluated at $r = 0$ and $\theta = 0$. We get

$$F_\perp(z,t) = I_1(z,t)\int dz_0 \frac{W_{1\perp}(z_0)}{v}e^{-j\omega\frac{z_0}{v}}. \tag{2.45}$$

We can define a transverse coupling impedance $Z_{1\perp}(\omega)$ as the work done to overcome this transverse force per unit charge per unit dipole current over a longitudinal length ℓ, or

$$\frac{Z_{1\perp}(\omega)}{\ell} = -\frac{1}{j\beta}\int d\tau W_{1\perp}(\tau)e^{-j\omega\tau}. \tag{2.46}$$

We would like $Z_{1\perp}$ to be real and positive in the case of a real loss. This occurs when the driving force $F_\perp$ is leading the dipole current I_1 by $\pi/2$, and therefore a factor of j is included in the denominator of Eq. (2.46). The factor of β is added to conform with the conventional definition. Here, $Z_{1\perp}$ is again the Fourier transform of the transverse wake field $W_{1\perp}$ just as $Z_{0\parallel}$ in Eq. (2.30) is the Fourier transform of the monopole longitudinal wake field $W_{0\parallel}$. Substituting the definition of $W_{1\perp}$ in Eqs. (2.38)-(2.40), we can write down the definition of the transverse impedance in general:

$$Z_{1\perp}(\omega) = \frac{1}{jI_1\beta_p}\int_0^\ell dz[(\mathbf{E}+(\boldsymbol{v}_p\times\mathbf{B})]_\perp. \tag{2.47}$$

As we have derived it here, from Eq. (2.43), v is the phase velocity of the current wave. But, just as for the longitudinal case, a dispersion relation will show that the phase velocity is not much different from the particle velocity, or the wave frequency $\omega \sim n\omega_0$ where $k = n/R$ and n is an harmonic number. However, for our dipole source ρ_1 of Eq. (2.4) and the dipole current wave of Eq. (2.43), we have not included an oscillation in the x-direction. This can be included by replacing $\cos\theta$

by $\cos(\theta - \nu\omega_0 t)$, where ν is the transverse tune or number of transverse oscillations made during one revolution of the storage ring. Then, the wave frequency of the dipole current in Eq. (2.43) changes from $\omega \sim n\omega_0$ to $\omega \sim (n \pm \nu)\omega_0$ and the phase velocity becomes

$$v_{phase} \sim \left(1 \pm \frac{\nu}{n}\right) v_p, \tag{2.48}$$

where v_p is the particle velocity. Thus, depending on the sizes of the tune ν and the harmonic number n, the phase velocity can be very much different from the particle velocity.

With the inclusion of the tune, corresponding to the dipole charge density source ρ_1 in Eq. (2.4), besides the dipole current density J_{z1} in Eq. (2.6), there are also current density components in the r and θ directions. The Maxwell equations can also be solved in the same way although they are very much more involved due to the nonvanishing r and θ components of the vector potential $\mathbf{A}$ and the more complicated expression of ∇^2 for these components. Nevertheless, the result is surprisingly simple; we get back exactly the same transverse impedance $Z_{1\perp}$ as Eq. (2.47) with the velocity being nearly the particle velocity. In other words, the tune does not contribute. This explains why the particle velocity has been written explicitly in Eq. (2.47).

Substituting Eq. (2.42) in Eq. (2.48), we finally obtain the space-charge contribution to the transverse impedance for the whole storage ring,

$$Z_{1\perp}(\omega) = -j\frac{Z_0 R}{\gamma_p^2 \beta_p^2}\left(\frac{1}{a^2} - \frac{1}{b^2}\right). \tag{2.49}$$

Note that the transverse impedance is defined as voltage per dipole current; therefore, it has a dimension of ohm/meter.

Again, the transverse space-charge impedance is important only in the situation of low particle velocity such as in the low-energy booster. The transverse space-charge wake force will modify the transverse tune of a particle at the edge of a coasting beam by

$$\Delta\nu = \frac{N r_p \bar{\beta}_x}{2\gamma_p^3 \beta_p^2 \pi}\left(\frac{1}{a^2} - \frac{1}{b^2}\right), \tag{2.50}$$

where N is the total number of particles in the beam, r_p the classical electromagnetic radius of the particle, and $\bar{\beta}_x$ the average beta function of the ring. This is called the direct space-charge tune shift and is directly related to $Z_{1\perp}$. There are also other contributions from the electric and magnetic images of the beam. Since the shift is different for particles at different deviations from the axis of the beam pipe, eventually a tune spread will be introduced. If this spread encircles any resonant region of the tune plot, the beam will be unstable. Thus, $Z_{1\perp}$ needs to be controlled.

Including wall impedance, the solution is altered to

$$Z_{1\perp}(\omega) = -j\frac{Z_0 R}{\gamma_p^2\beta_p^2}\left(\frac{1}{a^2}-\frac{1}{b^2}\right) + (1+j)\frac{2Rc}{\omega\sigma\delta b^3}, \tag{2.51}$$

where σ is the wall conductivity and δ the skin depth. We shall derive this term in the frequency domain later.

III PROPERTIES OF IMPEDANCES

The longitudinal and transverse impedances are introduced in the previous section to describe the wake fields in the frequency domain. However, it is obvious that both $Z_{0\parallel}$ and $Z_{1\perp}$ will not give a full description of the wake field left by a particle deviated from the axis of the beam pipe. For example, the dipole ring source also leaves behind a longitudinal electric field. Using Eqs. (2.14), (2.16) and (2.20), we obtain for the field,

$$E_z(r,\theta,z,t) = \int d\omega dk_z \frac{jk_z i_1 \delta(\omega - k_z v) R_1(qa) I_1(qr)\cos\theta}{2\pi^2\epsilon_0 q a^2 \gamma^2 D_1} e^{j(\omega t - k_z z)}. \tag{3.1}$$

This field is proportional to $r\cos\theta$ and will therefore affect a dipole following. From this longitudinal field we can define a dipole longitudinal wake field $W_{1\parallel}$ and hence a dipole longitudinal impedance $Z_{1\parallel}$. Instead of doing this one by one, we shall, in below, introduce the wake fields and the corresponding impedances for all multipoles.

First of all, by comparing E_z in Eq. (3.1) and the expression for the transverse force $F_\perp$ per unit charge in Eq. (2.39), we find

$$\frac{\partial E_z}{\partial r} = \frac{\partial F_\perp}{\partial z}. \tag{3.2}$$

This is the famous Panofsky-Wenzel theorem[2], which can be proved easily by expressing the electric field and the magnetic field in terms of the potential V and $\mathbf{A}$. Or, if we go to a frame where the magnetic field is zero, the theorem just spells $\nabla \times \mathbf{E} = 0$.

From Eqs. (2.17), (2.18) and (2.38), we know that

$$\tilde{E}_z \propto \tilde{V}, \tag{3.3}$$

and

$$\tilde{F}_\perp \propto \frac{\partial \tilde{V}}{\partial r}. \tag{3.4}$$

Using the general solution of $\tilde{V}$ for $r < a$ in Eq. (2.14), we can write, in general, for the fields at a distance $z_0 = vt - z$ behind the m-th multipole ring source $i_m = ea^m$ and near the axis of the beam pipe,

$$E_z(r, \theta, z_0) = -i_m W_{m\parallel}(z_0) r^m \cos m\theta, \tag{3.5}$$

$$F_\perp(r, \theta, z_0) = i_m W_{m\perp}(z_0) m r^{m-1} \cos m\theta. \tag{3.6}$$

Note that the definitions of the longitudinal and transverse wake fields for the m-th multipole $W_{m\parallel}$ and $W_{m\perp}$ conform with our previous definitions for the case of $m = 0$ and $m = 1$. Also note that $F_\perp$ in Eq (3.6) is in the x-direction. If the y-direction is preferred, one should replace all $\cos m\theta$ by $\sin m\theta$. Now, using the Panofsky-Wenzel theorem, we can easily relate the longitudinal and transverse wake fields for the same multipole; namely

$$W_{m\parallel}(z_0) = \frac{\partial}{\partial z_0} W_{m\perp}(z_0). \tag{3.7}$$

The corresponding impedances are defined as

$$\frac{Z_{m\parallel}(\omega)}{\ell} = \int d\tau W_{m\parallel}(\tau) e^{-j\omega\tau}, \tag{3.8}$$

and

$$\frac{Z_{m\perp}(\omega)}{\ell} = -\frac{1}{j\beta_p} \int d\tau W_{m\perp}(\tau) e^{-j\omega\tau}, \tag{3.9}$$

where $\tau = z_0/v$. The Panofsky-Wenzel theorem now reads

$$Z_{m\parallel}(\omega) = \frac{\omega}{c} Z_{m\perp}(\omega). \tag{3.10}$$

Note that the dimensions for $Z_{m\parallel}$ and $Z_{m\perp}$ are ΩL^{-2m} and ΩL^{-2m+1} respectively, while the dimensions for $W_{m\parallel}$ and $W_{m\perp}$ are $\Omega T^{-1} L^{-2m-1}$ and $\Omega T^{-1} L^{-2m}$ respectively.

The wake fields for all multipoles describe the fields left by a point charge in the time domain while the impedances for all the multipoles give an equivalent description in the frequency domain. In most problems, only the lowest multipoles are included. Therefore, we usually talk about only $Z_{0\parallel}$ and $Z_{1\perp}$, which are simply denoted by $Z_\parallel$ and $Z_\perp$, and neglect the rest. Although there is Eq. (3.10) that relates the longitudinal and transverse impedances for *the same* multipole, there is no relation, whatsoever, between the longitudinal and transverse impedances of *different* multipoles. In the literatures, some authors quote

$$Z_{1\perp}(\omega) = \frac{2c}{\omega b^2} Z_{0\parallel}(\omega). \tag{3.11}$$

This relation is strictly correct only for the wall impedances of a beam pipe of circular cross section but is totally incorrect for the space-charge effects as is evident when one compares Eqs. (2.35) and (2.51). However, it will usually give us some rough estimate of $Z_{1\perp}$ from $Z_{0\parallel}$, especially when $Z_{1\perp}$ is difficult to calculate.

We next study some properties of the wake fields and the impedances. These have been presented in detail in the lecture by Chao[1]. Here, we only review some important points that will be useful later. Only the space-charge effects are strongly dependent on the velocity of beam particles. These effects are in fact negligible for the SSC main ring where the particle velocity is essentially the velocity of light. As a result, in the following, unless specified otherwise, we shall treat all particles as having the velocity of light.

(i) Both the wake functions $W_{m\parallel}$ and $W_{m\perp}$ are real functions, from the Fourier transforms Eqs. (3.8) and (3.9), we get

$$Z^*_{m\parallel}(\omega) = Z_{m\parallel}(-\omega), \tag{3.12}$$

$$Z^*_{m\perp}(\omega) = -Z_{m\perp}(-\omega). \tag{3.13}$$

(ii) Since every particle is travelling with the velocity of light, due to causality, the wake fields $W_{m\parallel}(\tau)$ and $W_{m\perp}(\tau)$ are identically zero when τ is negative. From Eqs. (3.8) and (3.9), the impedances $Z_{m\parallel}(\omega)$ and $Z_{m\perp}(\omega)$, being Fourier transforms, can therefore be considered as analytic functions of ω in the lower half ω-plane with at most a singularity at $\omega = 0$. The real and imaginary parts of the impedances will then be related.

Consider a point $\xi = \omega - j\eta$ in the lower half ω-plane, $(\eta > 0)$. According to the Cauchy integral theorem, an impedance at ξ can be written as

$$Z(\xi) = -\frac{1}{2\pi j}\int dz Z(z)\left(\frac{1}{z-\xi} + \frac{1}{z-\xi^*}\right). \tag{3.14}$$

The closed contour of integration is shown in Fig. 3, which consists of going slightly below the real ω-axis and then around the lower half circle so that the point ξ is enclosed but not the possible singularity at $\omega = 0$. Note that the second term has no contribution because ξ^* is outside the contour. If $Z \to 0$ as $Im\,\omega \to -\infty$, the contribution of the lower half circle can be neglected and we have

$$Z(\xi) = -\frac{1}{\pi j}\int_{-\infty}^{\infty} dz \frac{(z-\omega)Z(z)}{(z-\omega)^2+\eta^2}. \tag{3.15}$$

We next let $\eta \to 0$ and arrive at

$$Re\,Z(\omega) = -\frac{\wp}{\pi}\int_{-\infty}^{\infty} d\omega' \frac{Im\,Z(\omega')}{\omega'-\omega}, \tag{3.16}$$

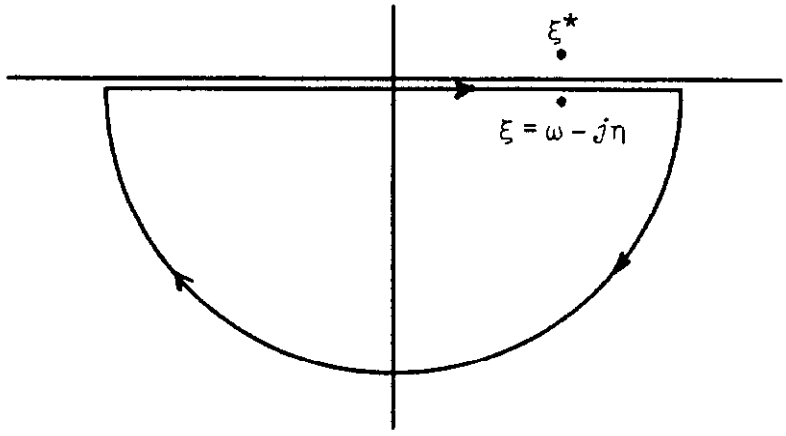

Figure 3: The complex ω-plane showing the poles and path of integration.

and

$$Im\, Z(\omega) = \frac{\wp}{\pi} \int_{-\infty}^{\infty} d\omega' \frac{Re\, Z(\omega')}{\omega' - \omega}, \tag{3.17}$$

where $\wp$ denotes the principal value and the two relations above are known as Hilbert transforms.

As an application, let us consider a narrow and sharp resonance,

$$Re\, Z_{\parallel}(\omega) = \frac{\pi R_s \omega_R}{2Q} [\delta(\omega - \omega_R) + \delta(\omega + \omega_R)], \tag{3.18}$$

where ω_R is the resonant frequency, R_s the shunt impedance, and Q the figure of merit. Here, we have simplified the problem by assuming $R_s \to \infty$ and $Q \to \infty$ but keeping R_s/Q constant. Using Eq. (3.17), the imaginary part can be obtained,

$$Im\, Z_{\parallel}(\omega) = \frac{R_s \omega_R}{2Q} \left(\frac{1}{\omega - \omega_R} + \frac{1}{\omega + \omega_R} \right). \tag{3.19}$$

We see that although $Re\, Z_{\parallel}$ has only two spikes at $\pm\omega_R$, $Im\, Z_{\parallel}$ is a continuum that has long tail attenuating very slowly like $1/\omega$.

In other cases, the evaluation of the principal values is sometimes rather difficult. Fortunately, the principal values can be avoided by using the fact that

$$\wp \int_{-\infty}^{\infty} \frac{d\omega'}{\omega' - \omega} = 0. \tag{3.20}$$

Then, the Hilbert transforms can be written without the singularities,

$$Re\, Z(\omega) = -\frac{1}{\pi}\int_{-\infty}^{\infty} d\omega' \frac{Im\, Z(\omega') - Im\, Z(\omega)}{\omega' - \omega}, \tag{3.21}$$

and

$$Im\, Z(\omega) = \frac{1}{\pi}\int_{-\infty}^{\infty} d\omega' \frac{Re\, Z(\omega') - Re\, Z(\omega)}{\omega' - \omega}. \tag{3.22}$$

Finally, we can simplify the integrals by noting the symmetries of the impedances when ω is changed to $-\omega$, namely Eqs. (3.12) and (3.13). The final results are: for the longitudinal impedances,

$$Im\, Z_{m\parallel}(\omega) = -\frac{2\omega}{\pi}\int_{0}^{\infty} d\omega' \frac{Re\, Z_{m\parallel}(\omega') - Re\, Z_{m\parallel}(\omega)}{\omega'^2 - \omega^2}, \tag{3.23}$$

$$Re\, Z_{m\parallel}(\omega) = \frac{2}{\pi}\int_{0}^{\infty} d\omega' \frac{\omega'\, Im\, Z_{m\parallel}(\omega') - \omega\, Im\, Z_{m\parallel}(\omega)}{\omega'^2 - \omega^2}, \tag{3.24}$$

and for the transverse impedances,

$$Im\, Z_{m\perp}(\omega) = \frac{2}{\pi}\int_{0}^{\infty} d\omega' \frac{\omega'\, Re\, Z_{m\perp}(\omega') - \omega\, Re\, Z_{m\perp}(\omega)}{\omega'^2 - \omega^2}, \tag{3.25}$$

$$Re\, Z_{m\perp}(\omega) = -\frac{2\omega}{\pi}\int_{0}^{\infty} d\omega' \frac{Im\, Z_{m\perp}(\omega') - Im\, Z_{m\perp}(\omega)}{\omega'^2 - \omega^2}. \tag{3.26}$$

Now let us examine, as an example, the wall impedances. From Eq. (2.36), the wall contribution is

$$Z_{\parallel}(\omega) = (1+j)\frac{R}{\sigma\delta b}, \tag{3.27}$$

where, if we go into the derivation, the factor $(1+j)$ comes from the square root of $j\omega$. In order that $Z_{\parallel}(\omega)$ is analytic in the lower half plane and the real part is positive since it is dissipative, we need to choose the sign of the square root so that

$$Z_{\parallel}(\omega) = -\left(\frac{\mu_0}{\sigma}\right)^{\frac{1}{2}}\left(\frac{R}{b}\right)|\omega|^{\frac{1}{2}}\, e^{j(\frac{\phi}{2}+\frac{\pi}{4})}, \tag{3.28}$$

where ϕ varying from π to 2π is the phase of ω. Thus, for real ω, the impedance reduces to

$$Z_{\parallel}(\omega) = [1 + \mathrm{sgn}(\omega)j]\left(\frac{\mu_0}{\sigma}\right)^{\frac{1}{2}}\left(\frac{R}{b}\right)\left|\frac{\omega}{2}\right|^{\frac{1}{2}}. \tag{3.29}$$

Note that this more careful definition conforms with the symmetry property of $Z_{\parallel}$ in Eq. (3.12). The contribution to the transverse impedance, from Eq. (2.51) is just proportional to $Z_{\parallel}(\omega)/\omega$. Therefore, for real ω, we have

$$Z_{\perp}(\omega) = [\mathrm{sgn}(\omega) + j]\left(\frac{mu_0}{\sigma}\right)^{\frac{1}{2}}\left(\frac{Rc}{b^3}\right)|\omega|^{-\frac{1}{2}}. \tag{3.30}$$

Since $Z_\perp(\omega) \to 0$ as $Im\,\omega \to -\infty$, we can verify the above Hilbert transforms. Since only real and positive ω is involved there, we can simplify Eq. (3.30) by writing

$$Z_\perp(\omega) = (1+j)a_\perp|\omega|^{-\frac{1}{2}}, \tag{3.31}$$

where $a_\perp$ is ω independent. Let us start with Eq. (3.26) by substituting $Im Z_\perp(\omega) = a_\perp|\omega|^{-1/2}$.

$$Re\, Z_\perp(\omega) = -\frac{2a_\perp\omega}{\pi}\int_0^\infty d\omega' \frac{\frac{1}{\sqrt{\omega'}} - \frac{1}{\sqrt{\omega}}}{\omega'^2 - \omega^2}. \tag{3.32}$$

This can be simplified by making the substitution $x = (\omega'/\omega)^{1/2}$ resulting in

$$Re\, Z_\perp(\omega) = -\frac{4a_\perp}{\pi\omega^{\frac{1}{2}}}\int_0^\infty dx \frac{1-x}{x^4-1}, \tag{3.33}$$

which can be easily integrated to give $Re\, Z_\perp(\omega) = a_\perp|\omega|^{-1/2}$ as required.

However, the same cannot be done with

$$Z_\parallel(\omega) = (1+j)a_\parallel|\omega|^{\frac{1}{2}} \tag{3.34}$$

for real and positive ω, where $a_\parallel$ is a constant. This is because, although $Z_\parallel$ is analytic in the lower half of the ω-plane, it does not go to zero when $Im\,\omega \to -\infty$. In other words, the contribution to the integration along the lower half circle in Eq. (3.14) does not vanish. If we substitute blindly $Re\, Z_\parallel(\omega) = a_\parallel|\omega|^{1/2}$ into Eq. (3.23), we get $Im\, Z_\parallel(\omega) = -a_\parallel|\omega|^{1/2}$ which is wrong. If we substitute $Im\, Z_\parallel(\omega)$ into Eq. (3.24), we find that the integral diverges.

For such an impedance, however, we can write a Hilbert transform for $Z_\parallel(\omega)/\omega$ instead, because $Z_\parallel(\omega)/\omega$ vanishes as $Im\,\omega \to -\infty$. But the symmetry property becomes

$$\left(\frac{Z_\parallel(\omega)}{\omega}\right)^* = -\left(\frac{Z_\parallel(-\omega)}{-\omega}\right), \tag{3.35}$$

which is the same as $Z_\perp(\omega)$. Therefore, the no-singularity relations (3.25) and (3.26) should hold. We know that this is indeed true because $Z_\parallel(\omega)/\omega$ has exactly the same ω dependence as $Z_\perp(\omega)$.

In using Hilbert transformation, one has to keep in mind that we may not be getting a unique result. This is because a frequency independent real impedance needs not have an imaginary counterpart. Also the *ideal* inductance or capacitance which gives rise to $Im\, Z_\parallel = \omega L$ or $-1/\omega C$ needs not have a real counterpart. In other words, to the $Im\, Z_\parallel$ obtained from $Re\, Z_\parallel$ through Hilbert transform, we can add any *ideal* inductive or capacitive terms. On the other hand, to the $Re\, Z_\parallel$

obtained from $Im\, Z_\parallel$ through Hilbert transform, we can add any pure frequency independent resistive term.

(iii) Consider a bunch whose m-th moment has a longitudinal distribution $\rho(z-ct)$. As it travels a distance ℓ, it gains energy at the rate of

$$\frac{d\epsilon}{dt} = c\int_{-\infty}^{\infty} dz\rho(z)\int_{z}^{\infty} dz'\rho(z')[-W_{m\parallel}(z'-z)]. \tag{3.36}$$

Note the negative sign in $-W_{m\parallel}$ which represents an accelerating field according to the definition in Eq. (3.5). In terms of the Fourier transform,

$$\tilde{\rho}(\omega) = \frac{1}{2\pi c}\int_{-\infty}^{\infty} dz\rho(z)e^{j\omega z/c}, \tag{3.37}$$

this rate of increase of energy is

$$\frac{d\epsilon}{dt} = -\frac{2\pi c^3}{\ell}\int_{-\infty}^{\infty} d\omega|\tilde{\rho}(\omega)|^2 Z_{m\parallel}(\omega). \tag{3.38}$$

Use has been made of Eq. (3.8) and the fact that the wake field $W_{m\parallel}(z)$ vanishes when $z<0$ so that the lower limit of the integral over dz' in Eq. (3.36) can be extended to $-\infty$. Since the charge density $\rho(z)$ is real, $|\tilde{\rho}(\omega)|^2$ is even in ω. According to the symmetry property of Eq. (3.12), the imaginary part of $Z_{m\parallel}(\omega)$ is odd in ω and does not contribute. Therefore, Eq. (3.38) can be written as

$$\frac{d\epsilon}{dt} = -\frac{4\pi c^3}{\ell}\int_{0}^{\infty} d\omega|\tilde{\rho}(\omega)|^2\, Re\, Z_{m\parallel}(\omega). \tag{3.39}$$

Since a beam as a whole cannot gain energy from the pipe structure, we conclude that

$$Re\, Z_{m\parallel}(\omega) \geq 0 \tag{3.40}$$

for all ω that is real, since $Re\, Z_{m\parallel}$ is even. Equation (3.10) then implies that

$$Re\, Z_{m\perp}(\omega) \geq 0 \tag{3.41}$$

when ω is real and positive, and

$$Re\, Z_{m\perp}(\omega) \leq 0 \tag{3.42}$$

when ω is real and negative.

Although impedances and wake functions give equivalent descriptions of the electromagnetic interaction between beam particles inside the beam pipe, in many cases impedances are preferred. This is because impedances are in the frequency

domain. In practice, a bunch has a distribution up to a finite frequency only. Thus, we only need to compute the impedances up to this frequency. Then, the effects of each frequency component can be studied.

We know of the concept of impedances through circuitry. Thus, the impedances of each discontinuity in the beam pipe can often be computed using equivalent circuits. For example, the effect of the beam pipe is equivalent to a wave guide. A sudden widening of the beam pipe is very nearly equivalent to a resonant cavity. Thus, the theories of wave guide and cavity can be employed in the estimation of the impedances.

We can compute the impedances of each discontinuity of the beam pipe and add them together. These will give an estimate for the total impedances of the whole accelerator ring. However, such additions assume that the discontinuities are so far separated that the fields inside them will not interfere with one another.

IV ESTIMATION OF IMPEDANCES

In this section, the impedances of some essential discontinuities of the vacuum chamber are computed. We shall try our best to work in the frequency domain without introducing the concept of wake functions. As a start, let us compute again the space-charge impedances. As it will be shown later, totally different approaches lead to the same results. After that, we shall tackle the problem of wall resistive impedances, the impedances for beam position monitors, bellows, kickers, and rf cavities.

Space-Charge

Consider a beam of radius a and current $I(t,z) = I_0 e^{jw(t-z/\beta c)}$ flowing along the axis of a circular beam pipe of radius b. The electric field E_0 seen by the beam can be computed using Faraday's law by integrating the electric field around a loop as in Fig. 4 and equating the result to the rate of change of magnetic flux linking the loop,

$$(E_0 + E_W)\Delta z + \Delta z \frac{\partial}{\partial z}\int E_r dr = -\frac{\partial}{\partial t}\int B_\theta dr \Delta z, \tag{4.1}$$

where the longitudinal length of the loop Δz is much less than the current wavelength $2\pi\beta c/\omega$. Then,

$$-E_0 = E_W - \frac{j\omega}{\beta c}\int E_r dr + j\omega \int B_\theta dr. \tag{4.2}$$

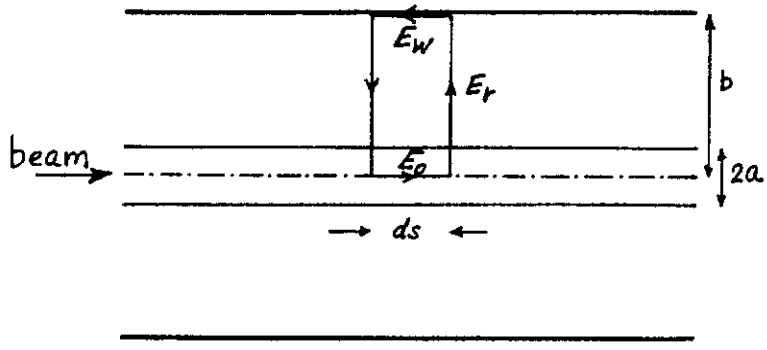

Figure 4: Derivation of space-charge impedance using Faraday's law.

We want to emphasize that βc is, as before, the phase velocity of the current wave, but is very nearly the particle velocity. The longitudinal impedance around the storage ring of radius R is therefore

$$Z_\parallel = -\frac{2\pi R E_0}{I_0}. \tag{4.3}$$

We have, by Ampere's law,

$$B_\theta = \frac{\mu_0 I_0 r}{2\pi a^2} \qquad r < a$$

$$B_\theta = \frac{\mu_0 I_0}{2\pi r} \qquad r > a, \tag{4.4}$$

and, by Gauss's law,

$$E_r = \frac{I_0/\beta c}{2\pi\epsilon_0}\frac{r}{a^2} \qquad r < a$$

$$E_r = \frac{I_0/\beta c}{2\pi\epsilon_0 r} \qquad r > a. \tag{4.5}$$

We first consider a perfectly conducting beam pipe so that the electric field at the inner surface of the wall is $E_W = 0$. We then have

$$-E_0 = -\frac{j\omega Z_0 I_0}{4\pi c}\left(\frac{1}{\beta^2} - 1\right) g_0, \tag{4.6}$$

where $g_0 = 2\ln(b/a) + 1$ is the same geometrical factor in Eq. (2.34). Therefore, the space-charge longitudinal impedance is

$$(Z_\parallel)_{sp} = -\left(\frac{j\omega R}{\beta c}\right)\left(\frac{Z_0 g_0}{2\beta\gamma^2}\right), \tag{4.7}$$

which is exactly the same as the space-charge contribution obtained in Eq. (2.33), although the present derivation is very much simpler and no Bessel functions are involved. The only restriction is that the wavelength of the current wave $2\pi\beta c/\omega$ in the center of mass-of-the beam particles is much bigger than the pipe radius, or $\omega \ll \gamma\beta c/b$. Equation (4.6) contains two terms: the first is the capacitive effect of the electric fields while the second, which is β^2 smaller, is the inductive effect of the magnetic fields. The space-charge contribution is just the sum of these two effects and therefore the presence of the factor γ^2 in the denominator of Eq. (4.7). When the phase velocity approaches c, the two effects cancel each other exactly. This explains why space-charge contribution is unimportant at high energies.

For the transverse space-charge impedance, let us study first the magnetic contribution. When the current deviates from the pipe axis by an amount $x_0 = \xi b$, the image surface current density at angle θ is

$$J(\theta; x_0) = -\frac{I_0}{2\pi b}\frac{1-\xi^2}{1+\xi^2-2\xi\cos\theta}. \tag{4.8}$$

This is obtained by the method of inversion by placing a current $-I_0$ at the point $x_1 = b^2/x_0$ as shown in Fig. 5. Then the beam pipe cylinder is an equipotential

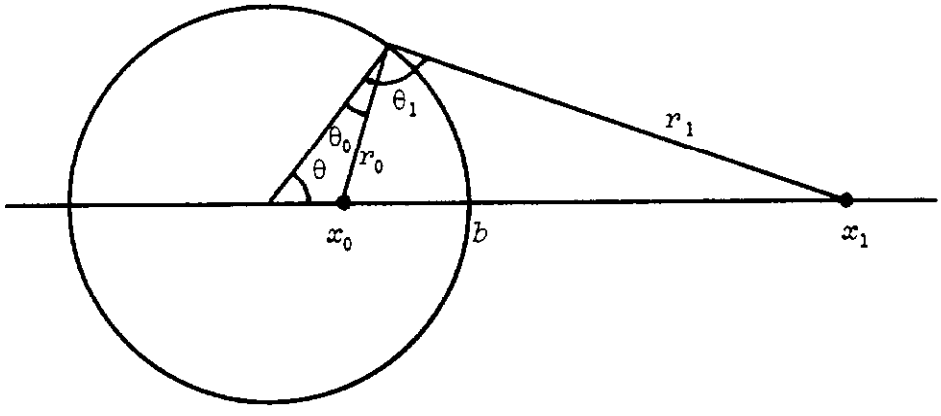

Figure 5: Computation of current density on cylinder using the method of inversion.

surface (using the analogy of a line charge). The image surface current density on the cylinder at angle θ can then be computed directly from the two current sources at x_0 and x_1:

$$J(\theta; x_0) = \frac{I_0}{2\pi}\left(\frac{\cos\theta_0}{r_0} - \frac{\cos\theta_1}{r_1}\right), \tag{4.9}$$

where r_0 and r_1 are distances from the point of observation to the current and its image respectively. Using the fact that $r_1 = br_0/x_0$, Eq. (4.9) leads to Eq. (4.8).

Since we are interested only in the dipole term, $J(\theta; x_0)$ can be expanded

$$J(\theta; x_0) = -\frac{I_0 x_0 \cos\theta}{\pi b^2}. \tag{4.10}$$

This current density in the wall of the beam pipe will produce at the pipe axis a vertical magnetic field,

$$B_y = -\int_0^{2\pi} d\theta \frac{\mu_o J \cos\theta}{2\pi b} = \frac{\mu_0 I_0 x_0}{2\pi b^2}, \tag{4.11}$$

which tries to deflect the beam more in the x-direction.

The actual unperturbed beam has a finite radius $a \gg x_0$ and is centered at the pipe axis. It carries a current density

$$J(r,\theta) = \frac{I_0}{\pi a^2} H(a-r), \tag{4.12}$$

where H is the step function. The horizontal deviation of the beam by a small amount x_0 leads to a perturbing current density

$$\begin{aligned} J(r,\theta)|_{x-x_0} - J(r,\theta)|_x &= -x_0 \left.\frac{\partial J(r,\theta)}{\partial x}\right|_{x=0} \\ &= \frac{I_0 x_0 \cos\theta}{\pi a^2}\delta(r-a), \end{aligned} \tag{4.13}$$

which resides solely on the beam surface and, exactly in the same manner as above, produces at the beam center a vertical magnetic self field,

$$B_y = -\frac{\mu_0 I_0 x_0}{2\pi a^2}. \tag{4.14}$$

Combining the magnetic contributions in Eqs. (4.11) and (4.14) and using the definition of $Z_\perp$ in Eq. (2.47), we obtain

$$(Z_\perp)_{mag} = jZ_0 R\left(\frac{1}{a^2} - \frac{1}{b^2}\right). \tag{4.15}$$

The electric part, which is $1/\beta_p^2$ times bigger and capacitive, can be included easily to give

$$(Z_\perp)_{sp} = -jZ_0 R\left(\frac{1}{\beta_p^2} - 1\right)\left(\frac{1}{a^2} - \frac{1}{b^2}\right), \tag{4.16}$$

which is the same as Eq. (2.49). Of course, if one likes, one can also work out the electric contribution in exactly the same way by thinking about charge distribution and radial electric field instead of current density and deflecting magnetic field.

For the SSC main ring, the ring radius $R = 13.201$ km and pipe radius $b = 1.65$ cm. The beam radius can be taken as $a = (\epsilon\beta^*/\gamma)^{1/2}$, where $\epsilon = 1 \times 10^{-6}$ m-rad is the normalized transverse emittance and β^* the beta function which has a minimum of 111 m. Thus, $(Z_\parallel)_{sp} = -j1.4 \times 10^{-3}\ \Omega$ at the injection energy of 1 TeV and $-j0.46 \times 10^{-5}\ \Omega$ at the final energy of 20 TeV. The transverse impedance is $(Z_\perp)_{sp} = -j21$ MΩ/m at 1 TeV and $-j1.1$ MΩ/m at 20 TeV.

Resistive Wall

From Eqs. (4.2) and (4.3), the wall resistivity contribution is given by the longitudinal electric field E_W at the inner surface of the beam pipe. The Maxwell's equations in the metallic wall of the beam pipe are:

$$\nabla \times \mathbf{H} = \sigma\mathbf{E} + j\omega\epsilon\mathbf{E},$$

$$\nabla \times \mathbf{E} = -j\omega\mathbf{B}, \tag{4.17}$$

where we have substituted the current density by $\mathbf{J} = \sigma\mathbf{E}$. For a conductive material such as stainless steel, the conductivity is $\sigma = 0.2 \times 10^7$ mho/m. Thus, when $\omega/2\pi \ll \sigma/2\pi\epsilon = 3.6 \times 10^{16}$ Hz, the displacement current $j\omega\epsilon\mathbf{E}$ can be safely neglected. In above, the electric permittivity ϵ in the metal has been approximated by its free-space value. Since the thickness Δ of the pipe wall is usually very much less than the pipe radius b, the pipe wall can be approximated by a metallic slab of thickness Δ, with normal pointing in the direction which we still designate by r. The Maxwell's equations then becomes

$$\frac{\partial^2 H_\theta}{\partial r^2} = j\omega\sigma\mu H_\theta,$$

$$E_z = \frac{1}{\sigma}\frac{\partial H_\theta}{\partial r}. \tag{4.18}$$

The solution inside the metallic slab is, for positive frequencies,

$$H_\theta = \mathcal{A}e^{-(1+j)r/\delta} + \mathcal{B}e^{(1+j)r/\delta},$$

$$E_z = -\frac{1+j}{\sigma\delta}\left[\mathcal{A}e^{-(1+j)r/\delta} - \mathcal{B}e^{(1+j)r/\delta}\right], \tag{4.19}$$

where $\delta = \sqrt{2/\mu\sigma\omega}$ is the skin depth, the depth into which the fields will penetrate if the thickness of the slab is infinite ($\mathcal{B} = 0$). Note that $|Z_0 H_\theta|$ is larger than $|E_z|$

by a factor of $Z_0\sigma\delta \gg 1$ ($Z_0\sigma\delta = 2.68 \times 10^3$ for stainless steel at 10 GHz) at least near the inner surface of the slab. After penetrating through the slab, the free-space Maxwell's equations are satisfied (with $\sigma = 0$ and the displacement current reinstated). However, such free-space solution is free-space radiation which requires $|Z_0 H_\theta| = |E_z|$. Thus, $Z_0 H_\theta$ needs to adjust itself so as to decrease sharply near the outer surface. As an approximation, we can set $Z_0 H_\theta = 0$ at the outer surface[3]. This will simplify the solution tremendously and the error introduced will be of the order $1/Z_0\sigma\delta$ only. With this approximation, we immediately get

$$\mathcal{B} = -\mathcal{A}\eta \tag{4.20}$$

with

$$\eta = e^{-2(1+j)\Delta/\delta}. \tag{4.21}$$

At the inner surface, Eq. (4.19) gives

$$E_z = -\frac{(1+j)}{\sigma\delta}\frac{1+\eta}{1-\eta}H_\theta. \tag{4.22}$$

For a beam current $I = I_0 e^{j\omega t}$ in the z-direction along the axis of the beam pipe, at the inner wall surface,

$$H_\theta = \frac{I_0}{2\pi b}. \tag{4.23}$$

We learn from Fig. 4 that $E_W = -E_z$. Then, according to Eq. (4.3), the longitudinal wall impedance for the whole storage ring is

$$(Z_\parallel)_{wall} = (1+j)\left(\frac{R}{\sigma\delta b}\right)\left(\frac{1+\eta}{1-\eta}\right). \tag{4.24}$$

When the beam pipe has a very thin wall, $\Delta \ll \delta$, η can be expanded and

$$(Z_\parallel)_{wall} = \frac{R}{\sigma\Delta b}. \tag{4.25}$$

This is just the dissipative resistance of the return current flowing through a slab of length $2\pi R$, width $2\pi b$, and thickness Δ. When the frequency is low enough, δ will be big and we will always be in this situation.

When the wall of the beam pipe has thickness $\Delta \gg \delta$, which is the situation when the frequency is large enough, η can be neglected and

$$(Z_\parallel)_{wall} = (1+j)\frac{R}{\sigma\delta b}. \tag{4.26}$$

In this case, the return current only penetrates a depth δ. Thus, Eq. (4.26) is just the impedance of a slab of length $2\pi R$, width $2\pi b$ and thickness δ. The inductive part comes about because the electromagnetic wave flowing into the walls of the beam pipe has to attenuate and, therefore, the wave number contains an imaginary part.

To compute the transverse impedance due to resistivity, we begin by displacing the beam current I horizontally from the pipe axis by an amount x_0. The image surface current density is given by Eq. (4.10), where we have kept only the dipole term. With a finite resistivity of the metallic wall, there is an electric field at the wall parallel to $J(\theta; x_0)$,

$$E_z(\theta; x_0) = (1+j)\frac{\mathcal{R}}{\delta} J(\theta; x_0), \tag{4.27}$$

where the surface resistivity $\mathcal{R}$ is related to the longitudinal electric field at the inner surface of the pipe wall in Eq. (4.22) and is defined as

$$\mathcal{R} = \frac{1}{\sigma}\left(\frac{1+\eta}{1-\eta}\right). \tag{4.28}$$

When the wall is infinitely thick, $\eta = 0$, and $\mathcal{R} = 1/\sigma$ is just the ordinary resistivity of the wall material. Elsewhere inside the pipe, $E_z(r, \theta; x_0)$ obeys

$$\left[\frac{1}{r}\frac{\partial}{\partial r}\left(r\frac{\partial}{\partial r}\right) - \frac{\omega^2}{\beta^2\gamma^2 c^2} - \frac{1}{r^2}\right] E_z(r, \theta; x_0) = 0. \tag{4.29}$$

Again, β and γ, although corresponding to the phase velocity of the wave, is very nearly the particle velocity when the beam is not oscillating transversely. Also, only the dipole term has been included. When $\omega \ll \beta\gamma c/b$, we get

$$E_z(r, \theta; x_0) = -(1+j) I_0 \frac{\mathcal{R}}{\delta} \frac{x_0 r \cos\theta}{\pi b^3}. \tag{4.30}$$

Now we place another current $-I$ at $-x_0$ so as to form a beam dipole. For small x_0, the longitudinal electric field due to the resistivity of the wall can be obtained by differentiating Eq. (4.30):

$$\begin{aligned} E_z(r, \theta) &= \frac{\partial E_z(r, \theta; x_0)}{\partial x_0}(2x_0) \\ &= 2 I_0 x_0 \frac{\mathcal{R}}{\delta} \frac{r\cos\theta}{\pi b^3}. \end{aligned} \tag{4.31}$$

This longitudinal electric field produces through Faraday's law a transverse magnetic field,

$$B_\perp(r,\theta) = -\frac{1}{j\omega}\nabla_\perp \times E_z. \tag{4.32}$$

At the beam dipole, $r = 0$, we get

$$B_y = -(1+j)\frac{2I_0 x_0 \mathcal{R}}{j\omega\delta\pi b^3}, \tag{4.33}$$

which tends to enlarge the separation between the dipole currents. According to the definition of Eq. (2.47) and remembering that the beam separation is $2x_0$, the transverse impedance due to wall resistivity of the whole ring is

$$(Z_\perp)_{wall} = (1+j)\frac{2Rc\mathcal{R}}{\omega\delta b^3}, \tag{4.34}$$

which is the same as given in Eq. (2.51) and is related to the longitudinal wall impedance by Eq. (3.11).

The transverse wall impedance can drive coupled-bunch instabilities with growth rate for the μ-th mode without Landau damping[1],

$$\frac{1}{\tau_\mu} = -\frac{eMI_b c}{4\pi\nu E}\sum_{k=-\infty}^{\infty} Re\, Z_\perp[(kM-\mu+\nu)\omega_0], \tag{4.35}$$

where M is the number of bunches, I_b the average current of one bunch, ν the transverse betatron tune, and $\omega_0/2\pi$ the revolution frequency. Since $Re\, Z_\perp \propto \omega^{-1/2}$ and is positive (negative) when ω is positive (negative), a small negative ω spectral line can cause an instability. For the SSC, $M = 17100$, $\nu = 78.28$. The mode $\nu = 79$ will have spectral lines at $-17100.72\omega_0$, $-0.72\omega_0$, $17099.28\omega_0, \ldots$. The line at $-0.72\omega_0$ will lead to a growth, while the other lines do not contribute essentially to the summation of Eq. (4.35) as illustrated in Fig. 6.

A proposal to reduce the growth is to coat the inner surface of the pipe wall with a highly conductive layer; for example, copper whose conductivity is ~ 30 times bigger at 4°K than at room temperature. The reduction of the resistive wall impedance will lower the parasitic heating also. At the same time, such a copper layer will also shield the beam from any possible high-frequency variations in external magnetic field. It is also preferred in order to minimize the eddy current effects during a magnet quench.

To compute the impedance of such a beam pipe, we again approximate it by a slab with two layers; the inner one has thickness Δ_1 and conductivity σ_1 while

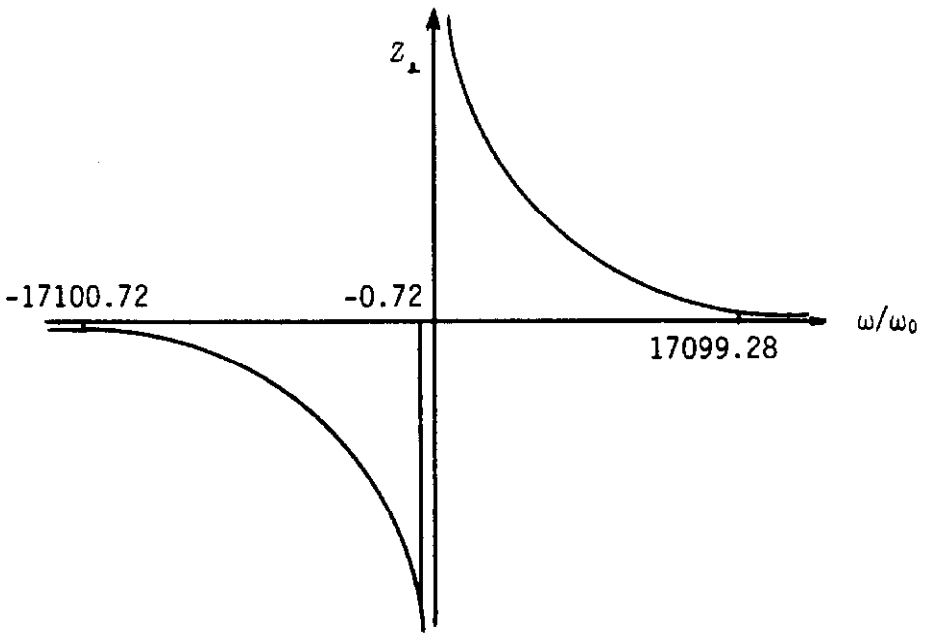

Figure 6: Plot of $(Z_\perp)_{wall}$ and the spectral lines of a bunch at low frequencies.

the outer one has thickness Δ_2 and conductivity σ_2. The solution to the Maxwell's equations is

$$H_\theta = \mathcal{A}_i e^{-(1+j)r/\delta_i} + \mathcal{B}_i e^{(1+j)r/\delta_i},$$
$$E_z = -\frac{1+j}{\sigma_i}\left[\mathcal{A}_i e^{-(1+j)r/\delta_i} - \mathcal{B}_i e^{(1+j)r/\delta_i}\right], \tag{4.36}$$

where $i = 1$ is inside the first layer or $0 < r < \Delta_1$ and $i = 2$ is inside the outer layer or $\Delta_1 < r < \Delta_1 + \Delta_2$. Again, we make the approximation that[3] $H_\theta = 0$ at $r = \Delta_1 + \Delta_2$ after penetrating both layers. We next invoke the continuity of H_θ and E_z at $r = \Delta_1$ and the fact that $H_\theta = I/2\pi b$ at $r = 0$. Then, all the unknowns $\mathcal{A}_i$ and $\mathcal{B}_i$ can be determined and so is the longitudinal wall impedance

$$(Z_\parallel)_{wall} = (1+j)\frac{R}{\sigma_1\delta_1 b}\varsigma, \tag{4.37}$$

where

$$\varsigma = \frac{1 + \left(\frac{\sigma_2}{\sigma_1}\right)^{1/2}\left(\frac{1-\eta_1}{1+\eta_1}\right)\left(\frac{1-\eta_2}{1+\eta_2}\right)}{\left(\frac{1-\eta_1}{1+\eta_1}\right) + \left(\frac{\sigma_2}{\sigma_1}\right)^{1/2}\left(\frac{1-\eta_2}{1+\eta_2}\right)} \tag{4.38}$$

and

$$\eta_i = e^{-2(1+j)\Delta_i/\delta_i}. \tag{4.39}$$

Various familiar results emerge by taking appropriate limits:
(a) $\Delta_2 = 0$. Then, $\eta_2 \to 1$ and $\varsigma = (1+\eta_1)/(1-\eta_1)$. We get back Eq. (4.24) for just one layer of metallic medium.
(b) $\Delta_1 = 0$. Then

$$\varsigma = \left(\frac{\sigma_1}{\sigma_2}\right)^{\frac{1}{2}} \left(\frac{1+\eta_2}{1-\eta_2}\right), \tag{4.40}$$

which gives the same formula as in Case (a) with $1 \to 2$, the factor $(\sigma_1/\sigma_2)^{1/2}$ being necessary to convert $1/\sigma_1\delta_1$ to $1/\sigma_2\delta_2$ in Eq. (4.24).
(c) $\Delta_1 \gg \delta_1$. Then, $\eta_1 \to 0$ and $\varsigma = 1$. We get back the impedance for one thick layer regardless of Δ_2 and σ_2.
(d) $\Delta_2 \gg \delta_2$. Then, $\eta_2 \to 0$ and

$$\varsigma = \frac{1 - \left(\frac{1-\sqrt{\sigma_1/\sigma_2}}{1+\sqrt{\sigma_1/\sigma_2}}\right)\eta_1}{1 + \left(\frac{1-\sqrt{\sigma_1/\sigma_2}}{1+\sqrt{\sigma_1/\sigma_2}}\right)\eta_2}, \tag{4.41}$$

which is the result given by Ng[4] for an infinitely thick outer layer.
(e) Very low frequencies. Then, both Δ_1/δ_1 and Δ_2/δ_2 are small and η_1 and eta_2 can be expanded. The final result is very simple and is just a modification of Eq (4.25),

$$(Z_\parallel)_{wall} = \frac{R}{b}\frac{1}{\sigma_1\Delta_1 + \sigma_2\Delta_2}.$$

The transverse impedance is again given by Eq. (4.34) with the surface resistivity $\mathcal{R} = \varsigma/\sigma_1$.

Coming back to the transverse coupled-bunch instabilities, the lowest frequency of concern is $(\mu - \nu)\omega_0$. Without much constraint on the tune choice, let us take $\mu - \nu$ to be 0.1, for which the cold copper and stainless steel skin depths are 0.63 mm and 19 mm respectively. For the present pipe design, $\Delta_1 = 0.1$ mm and $\Delta_2 = 1$ mm. We obtain $\varsigma = (2.98 - j2.87)$ and a growth time of 8.5 ms at 1 TeV. The growth rate would be 100 times faster if the 1 mm stainless steel pipe were not copper coated. We show in Fig. 7 the longitudinal and transverse wall impedances given by the formulae above. The copper layer thickness corresponds to a wavelength at frequency $\omega = 83.8$ kHz. Above that, the return current resides in the thin copper coating only and the impedances are $Z_\parallel/n = (1+j)2.24n^{-1/2}\ \Omega$ and $Z_\perp = (1+j)218n^{-1/2}$ MΩ/m. At very low frequencies, $\mathcal{R}e(Z_\parallel/n) = 4.40/n\ \Omega$ and $\mathcal{R}e(Z_\perp) = 427/n$ MΩ/m. The imaginary parts are a few orders of magnitude smaller.

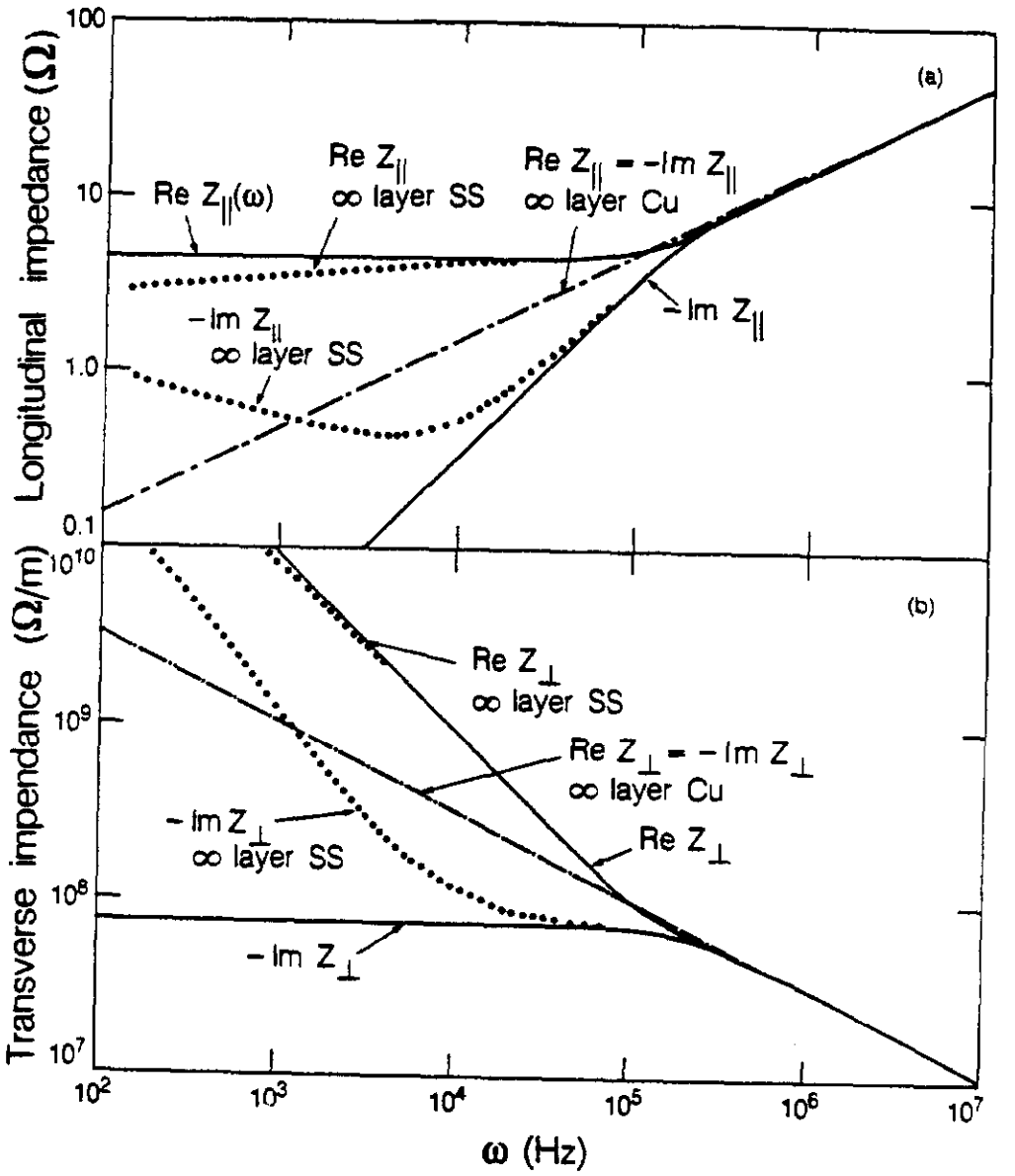

Figure 7: The solid curves are the SSC resistive wall impedance with parameters stated in text. For comparison, the dotted (dashed) curves are for the stainless steel (copper) layer infinitely thick.

Beam Position Monitors

Beam position monitors are required to measure the horizontal and vertical positions of the beam so that it can be guided through the central region of a beam pipe of $\sim$ 1.65 cm radius and circulate around the storage ring many many times. Since beam signals are registered at the terminations, the monitors must exhibit impedances to the beam.

The beam monitors that will be discussed here are cylindrical stripline pickups, primarily because the computations are usually much simpler than the rectangular geometry ones. However, in many cases, for example, the Fermilab main ring, the rectangular geometry is preferred over cylindrical. Hopefully, our cylindrical results below would provide at least a rough estimation for the rectangular counterpart.

Consider a pair of cylindrical stripline pickups[5] exposed to a short beam bunch as shown in Fig. 8(a). Each stripline has a length ℓ and subtends an angle ϕ_0 to the beam pipe axis. The stripline together with the extruded beam pipe behind it can be considered as a section of transmission line with a characteristic impedance $Z_s = \sqrt{L/C}$, where L and C are the inductance and capacitance per unit length. Any signal propagating along this section of transmission line will have a velocity $\beta_s c = 1/\sqrt{LC}$. Each end of the stripline is attached via a port to a transmission line of the same characteristic impedance. Hence, any signal induced on the stripline will either propagate through one of the ports onto a transmission line without reflections. This is just equivalent to terminating each end of the stripline by a resistance of Z_s as in Fig. 8(b).

When a beam bunch of time distribution $I(t)$ and velocity $\beta_p c$ traveling along the axis of the beam pipe crosses the first or upstream port, the image current on the walls of the pipe sees an impedance of $Z_s/2$, representing the parallel impedance of the upstream termination impedance Z_s and the transmission line formed by the stripline which, since terminated at the far end by Z_s, also has impedance Z_s. In other words, the image current splits into two equal parts, one traveling through the upstream termination and detected while the other half travels along the stripline and ends up going through the downstream termination a time $\ell/\beta_s c$ later.

When the bunch beam passes through the downstream port the same thing happens but the polarity reverses. One half of the signal will travel through the downstream termination while the other half propagates up the stripline to be collected by the upstream termination. Thus, the voltage across the upstream termination is

$$V_u(t) = \frac{Z_s}{2}\left(\frac{\phi_0}{2\pi}\right)\left[I(t) - I\left(t - \frac{\ell}{\beta_p c} - \frac{\ell}{\beta_s c}\right)\right], \tag{4.42}$$

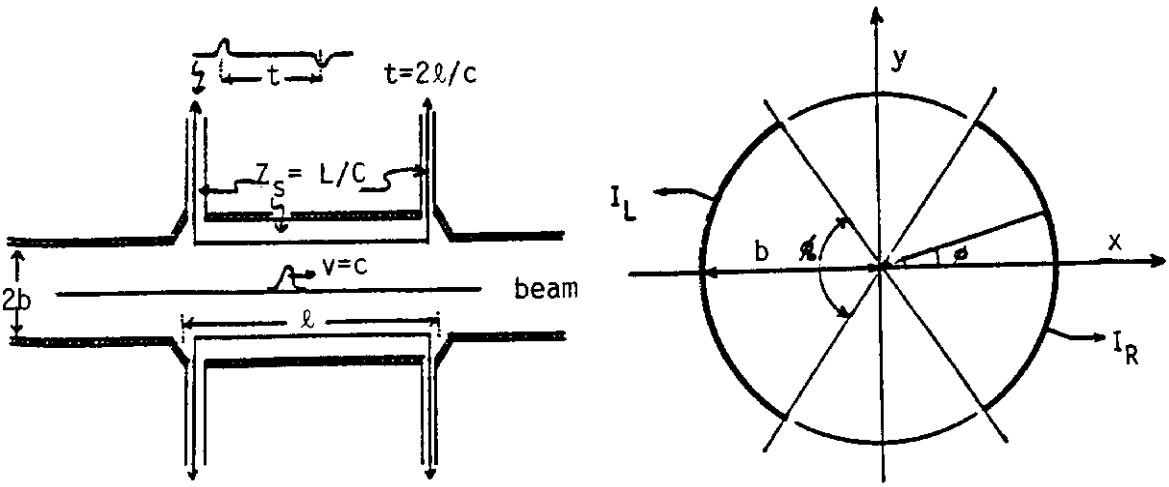

(a)

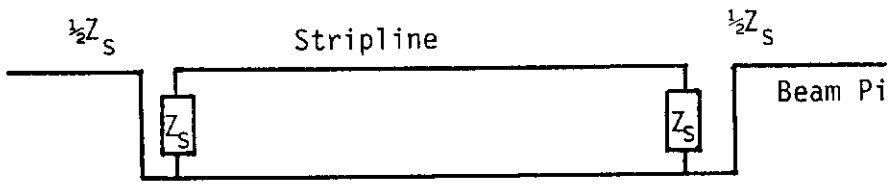

(b)

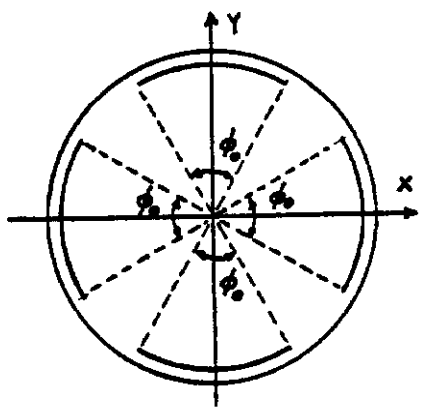

(c)

Figure 8: Beam position monitor. (a) Geometry of cylindrical stripline monitor. (b) A stripline forming a transmission line with the beam pipe having characteristic impedance Z_0 and terminated at both ends by Z_s. (c) The SSC 4-electrode monitor.

and that across the down stream termination is

$$V_d(t) = \frac{Z_s}{2}\left(\frac{\phi_0}{2\pi}\right)\left[I\left(t-\frac{\ell}{\beta_s c}\right) - I\left(t-\frac{\ell}{\beta_p c}\right)\right]. \tag{4.43}$$

The factor $\phi_0/2\pi$ comes about because only such a fraction of the image current will flow through a port.

The net signal seen at the upstream port is a bipolar doublet with each lobe having essentially the same time distribution as the beam bunch itself but separated by a constant time of $(\ell/\beta_p c + \ell/\beta_s c)$. However, the signal at the downstream port will be completely cancelled if the beam velocity and the signal velocity are the same. This is, in fact, the situation, since the signal velocity in a transmission line with a free-space medium is exactly c and the beam particle velocity is also very close to c. For simplicity, we shall set $\beta_p = \beta_s = 1$ in below and forget the downstream port.

In the frequency domain, the beam has a current $I(t) = I_0 e^{j\omega t}$ at the upstream port. Note that I_0 is in general complex but is time independent. The voltage across the upstream port becomes

$$V_u(\omega) = \frac{Z_s}{2}\left(\frac{\phi_0}{2\pi}\right) I_0\left(1 - e^{j2\omega\ell/c}\right). \tag{4.44}$$

This happens to be also the potential difference across the gap at the upstream end. The total image current in the walls of the beam pipe is, of course $-I_0$. But only a fraction $\phi_0/2\pi$ will see this potential difference while the rest just flow through without meeting any resistance. As a result, the *average* potential seen by the particle beam is

$$V_b(\omega) = \left(\frac{\phi_0}{2\pi}\right) V_u(\omega). \tag{4.45}$$

The longitudinal impedance for one strip plate is therefore $(Z_\parallel)_{BPM} = V_b(\omega)/I_0$, or

$$(Z_\parallel)_{BPM} = Z_s\left(\frac{\phi_0}{2\pi}\right)^2\left(\sin^2\frac{\omega\ell}{c} + j\sin\frac{\omega\ell}{c}\cos\frac{\omega\ell}{c}\right). \tag{4.46}$$

The same impedance can be computed using Eq. (4.44) in another way. The average real power dissipated in the upstream termination is

$$P(\omega) = \frac{|V_u(\omega)|^2}{2Z_s}. \tag{4.47}$$

This is by definition equal to $\frac{1}{2}|I_0|^2\, \mathcal{R}e(Z_\parallel)_{BPM}$, which results in the same $\mathcal{R}e(Z_\parallel)_{BPM}$ as Eq. (4.46). The imaginary part can be obtained using Hilbert transformation

and is left as an exercise for the reader. However, in this situation, $Re\, Z_\parallel(\omega)$ does not vanish at infinity and we have to work with $Re\, Z_\parallel(\omega)/\omega$ instead.

Note that the longitudinal impedance starts out inductively at low frequencies and, after $\omega = \pi c/2\ell$, alternates between capacitive and inductive. However, there are no sharp resonances since the stripline is match-terminated at both ends. There are some striplines, like those in the Fermilab Main Ring, that have one match-termination only at the center. The impedance seen at each end is Z_s in parallel with an open transmission line of characteristic impedance of Z_s. At low frequencies, the impedance seen is, therefore, just Z_s, and the currents from each end of the stripline will be absorbed totally without any reflection. However, this is not true at high frequencies, because the stripline can accept resonances with standing waves having a node at the middle where the termination does not absorb any power and the resonances will not be disturbed. Such beam position monitors are analyzed and the coupling impedance computed in Part II of this book.

Let us turn to the problem of transverse coupling impedance. Assume a dipole current source separated by Δ; i. e., I at $x = \Delta/2$ and $-I$ at $x = -\Delta/2$. Here, we assume that the pair of cylindrical striplines are positioned horizontally as in Fig. 8(a). Note that both currents have the same t and z dependence, such as $e^{j\omega(t-x/\beta c)}$, so that both are traveling in the same direction, or only the upstream termination will see a signal. From Eq. (4.10), the current flowing into the right stripline system is, keeping only up to the dipole term,

$$I_R = \int_{-\phi_0/2}^{\phi_0/2} -\frac{I_0 \Delta \cos\theta}{\pi b^2} b d\theta, \tag{4.48}$$

and the current flowing into the left stripline system is

$$I_L = -I_R. \tag{4.49}$$

Using Eq. (4.44), the voltages at the right and left upstream gaps are, respectively,

$$V_R = Z_s \frac{I_0 \Delta}{\pi b} \sin\frac{\phi_0}{2} \left(1 - e^{j2\omega\ell/c}\right),$$
$$V_L = -V_R. \tag{4.50}$$

The total average power dissipated is

$$P = \frac{1}{2Z_s}(|V_L|^2 + |V_R|^2), \tag{4.51}$$

or

$$P = 4Z_s \left(\frac{|I_0|\Delta}{\pi b}\right)^2 \sin^2\frac{\phi_0}{2} \sin^2\frac{\omega\ell}{c}. \tag{4.52}$$

There is a relation between the power dissipated and the real part of the transverse impedance derived by Nassibian and Sacherer[6] which we are going to repeat here. For a length ℓ of current loop, the interaction with the beam detector will give a magnetic field B_y through the loop so a back e.m.f. will be induced. Equivalently, the current in the loop will see an impedance Z given by

$$j\omega B_y \ell \Delta = Z I_0. \tag{4.53}$$

Substituting into the definition of $Z_\perp$ of Eq. (2.47) gives a horizontal transverse impedance,

$$Z_\perp = \frac{cZ}{\omega \Delta^2}. \tag{4.54}$$

The power dissipated is $P = \frac{1}{2}|I_0|^2 \, \mathcal{R}e\, Z$ and we therefore get

$$P = \frac{1}{2}\frac{\omega}{c}(I_0 \Delta)^2 \, \mathcal{R}e\, Z_\perp. \tag{4.55}$$

Thus, for a pair of striplines

$$\mathcal{R}e(Z_\perp)_{BPM} = \frac{8Z_0}{\pi^2 b^2}\frac{c}{\omega}\sin^2\frac{\phi_0}{2}\sin^2\frac{\omega\ell}{c}, \tag{4.56}$$

which has exactly the same frequency dependence as $\mathcal{R}e(Z_\parallel)_{BPM}/\omega$. The imaginary part can be found by Hilbert transform; it should have exactly the same frequency dependence as $\mathcal{I}m(Z_\parallel)_{BPM}/\omega$. Therefore, for a pair of striplines

$$(Z_\perp)_{BPM} = \frac{c}{b^2}\left(\frac{4}{\phi_0}\right)^2 \sin^2\frac{\phi_0}{2}\frac{(Z_\parallel)_{BPM}}{\omega} \qquad \perp \text{to striplines} \tag{4.57}$$

or the x-direction here. In above, $(Z_\parallel)_{BPM}$ is the longitudinal coupling impedance of also a pair of *two* striplines.

To compute the transverse impedance in the y-direction, we put the currents I at $y = \Delta/2$ and $-I$ at $y = -\Delta/2$ instead. Then the current flowing into the right stripline system is

$$I_R = \int_{-\phi_0/2}^{\phi_0/2} -\frac{I_0 \Delta \cos(\frac{\pi}{2}+\theta)}{2\pi b^2} b d\theta, \tag{4.58}$$

which is identically zero and so is also I_L. The voltages across each upstream gap are therefore also zero. Thus,

$$(Z_\perp)_{BPM} = 0 \qquad \parallel \text{ to striplines} \tag{4.59}$$

or the y-direction here. The reason is clear, because $(Z_\perp)_{BPM}$ depends on the voltages across the striplines gap which, in turn, depend only on the *total* currents

flowing across each gap but not on the actual distribution of the current density. However, a current dipole at $y = \pm\Delta/2$ will only produce image current distribution that is antisymmetric with respect to the x-axis while the *total* currents crossing each gap are zero.

In the SSC, the most demanding requirement for the beam position monitors is in the commissioning stage where very low beam currents must be used in order not to quench the magnets. It appears that both coordinates must be measured at every quadrupole (one per half cell); so the pickups must be a 4-electrode design shown in Fig. 8(c). We take[7] $\phi_0 = 55°$, $\ell = 10$ cm, and $Z_s = 50$ ohms. The pipe radius is $b = 1.65$ cm. At low frequencies, $\omega/2\pi \ll c/4\ell = 750$ MHz, the longitudinal impedance per harmonic per monitor (*four* striplines) is

$$\left(\frac{Z_\parallel}{n}\right)_{BPM} = jZ_s\left(\frac{\phi_0}{\pi}\right)^2\frac{\ell}{R} = 3.53\times 10^{-5}\ \Omega, \tag{4.60}$$

while the transverse impedance is (only *two* striplines are contributing, either in the x-direction or the y-direction),

$$(Z_\perp)_{BPM} = j\frac{8Z_s\ell}{\pi^2 b^2}\sin^2\frac{\phi_0}{2} = 3.17\ \text{k}\Omega/\text{m}. \tag{4.61}$$

With almost 900 sets of monitors in each ring, the impedances are $(Z_\parallel/n)_{BPM} \sim j0.0318\ \Omega$ and $(Z_\perp)_{BPM} \sim j2.86\ \text{M}\Omega/\text{m}$ for either the horizontal or vertical direction.

We can also compute the longitudinal impedance of a beam passing through a pair of striplines shown in Fig. 8(a) but deviated from the central axis by x_0 horizontally and y_0 vertically. Using Eq. (4.8), the total image currents flowing across the right and left upstream gaps are:

$$I_{R,L} = -I_0\left(\frac{\phi_0}{2\pi}\right)\left[1 \pm \frac{4x_0}{b}\frac{\sin(\phi_0/2)}{\phi_0} + \frac{2(x_0^2 - y_0^2)}{b^2}\sin\phi_0\right]. \tag{4.62}$$

Note that the second term is the dipole term and we have included a third term that is of a higher multipole. In the present situation, it is not so simple to compute the *average* voltage seen by the particle beam because the beam has been displaced and the distribution of the image current is no longer uniform. As a result, we will compute the power dissipated at the upstream terminations and infer the real part of the longitudinal impedance. This power is proportional to the sum of $|I_R|^2$ and $|I_L|^2$ and is given by

$$P_{disp} = 2G(x_0, y_0)P, \tag{4.63}$$

where P is the power dissipated through *one* stripline when the beam is at the central axis of the beam pipe as given by Eq. (4.47), and the function

$$G(x_0, y_0) = 1 + \left(\frac{x_0}{b}\right)^2 \left(\frac{4}{\phi_0}\right)^2 \sin^2 \frac{\phi_0}{2} + \left(\frac{x_0^2 - y_0^2}{b^2}\right) \left(\frac{4}{\phi_0}\right) \sin \phi_0 \tag{4.64}$$

takes care of the fact the the beam is displaced. The longitudinal impedance of a pair of striplines is therefore equal to $G(x_0, y_0)$ times the impedance of an undisplaced beam. Note that the second term of $G(x_0, y_0)$ comes from the square of the dipole term while the third term is from the higher multipole. Here, the term linear in x_0 or the linear dipole term cancels out. This is, in fact, exactly what we expect. In order to measure the deviation of the beam from the central axis, one should measure the difference between the left and right terminations but not the sum; then, the linear dipole term will emerge.

The longitudinal coupling impedance of a displaced beam provides a way to compute the transverse coupling impedances[6]. This method is very useful, so we will derive it here. Let us concentrate on displacement in the x-direction only. We write $E_z(x, x_0)$ as the image electric field at x due to a current I at x_0. For a length ℓ, define

$$Z_\parallel(x, x_0) = \frac{\ell E_z(x, x_0)}{I}, \tag{4.65}$$

which is a measurable quantity and reduces to the usual longitudinal impedance $Z_\parallel(x_0)$ at x_0 in the limit $x \to x_0$.

The image electric field at x due to a dipole current at x_0 separated by Δ is

$$E'_z = \frac{\partial E_z(x, x_0)}{\partial x_0} \Delta, \tag{4.66}$$

and the magnetic field at x perpendicular to the plane of the dipole is, by Faraday's law,

$$B'_y = \frac{\Delta}{j\omega} \frac{\partial^2 E_z(x, x_0)}{\partial x \partial x_0}. \tag{4.67}$$

Substituting into the definition of $Z_\perp$ of Eq. (2.47), the horizontal transverse impedance displaced by x_0 is

$$Z_\perp = \frac{c}{\omega} \left. \frac{\partial^2 Z_\parallel(x, x_0)}{\partial x \partial x_0} \right|_{x=x_0}. \tag{4.68}$$

The vertical transverse impedance can be inferred similarly.

In many cases, the longitudinal impedance at (x_0, y_0) has the form

$$Z_\parallel(x_0, y_0) = [1 + F_x^2(x_0) + F_y^2(y_0)]\, Z_\parallel\big|_{x_0=0, y_0=0}; \tag{4.69}$$

so $Z_\perp$ can be obtained directly from the position dependence of $Z_\parallel$. For example, the horizontal transverse impedance is

$$Z_\perp = \frac{c}{\omega}\left(\frac{dF_x}{dx_0}\right)^2 Z_\parallel\Big|_{x_0=0,y_0=0}. \tag{4.70}$$

However, one should be careful that only dipole contributions should be included into F_x and F_y since the dipole impedances cannot receive contributions from other multipoles. In our situation, the square bracketed term in Eq. (4.69) is just the function $G(x_0, y_0)$ in Eq. (4.64) but with the higher multipole term removed (keeping only the second term). Then, substitution into Eq. (4.70) will lead to exactly the same transverse impedances we obtained earlier in Eqs. (4.57) and (4.59).

Bellows

Between sections of the vacuum chamber, bellows are needed to compensate for thermal expansion and transverse offsets. Roughly speaking[8], the ratio of compression and extension to length for bellows is of the order of $\sim 30\%$. The average coefficient of expansion for stainless steel from 0°K to 300°K is $\sim 14.5\times10^{-6}/°\mathrm{K}$. Therefore, for the SSC, which has a circumference of 82.944 km, ~ 1.20 km ($\sim 1.45\%$)of bellows are needed. Such a length of bellows will certainly contribute to the longitudinal and transverse impedances of the storage ring and will therefore affect the stability of the beam.

To study the bellows, let us begin by examining one *rectangular* corrugation of the bellows. Let b be the radius of the beam pipe, Δ and $2g$ be respectively the depth and width of the corrugation. Henke[9] has studied the problem in the frequency domain, which involves the solution of an infinite matrix equation. This complicated equation can be simplified[10] in the case when $g/b \ll 1$. The longitudinal impedance of such a corrugation becomes,

$$Z_\parallel(\omega) = \frac{gZ_0}{\pi b I_0^2(\bar{b})D}, \tag{4.71}$$

where

$$D = j\frac{R_0'(kb)}{R_0(kb)} - 2kj\left[\sum_{s=1}^{S}\frac{1}{\beta_s^2}\left(1-e^{-j\beta_s g}\frac{\sin\beta_s g}{\beta_s g}\right) - \sum_{s=S+1}^{\infty}\frac{1}{\alpha_s^2}\left(1-e^{-\alpha_s g}\frac{\sinh\alpha_s g}{\alpha_s g}\right)\right]. \tag{4.72}$$

In the above, $k=\omega/c$, $Z_0 = 377\ \Omega$, I_0 is the modified Bessel function of order zero, $\bar{b} = bk/\gamma\beta$, γ and β are the relativistic velocity parameters of the beam particles. In the summations, $\beta_s = \sqrt{(k^2b^2 - j_{os}^2)}$ and $\alpha_s = \sqrt{(j_{0s}^2 - k^2b^2)}$, where j_{0s} is the s-th

zero of the Bessel function J_0 and j_{0S} is the zero that is just larger or equal to kb. Also, $R(kb) = J_0(kb)N_0(kd) - J_0(kd)N_0(kb)$, where $d = b + \Delta$ and J_0 and N_0 are respectively the Bessel function and Neumann function of order zero. To have a deeper insight, let us take the limit $kb \gg 1$ and $g \to 0$, then, by expanding the sine, sinh and the exponentials, D can be simplified to

$$D = -j \cot k\Delta + 2kg \left(\sum_{s=1}^{S} \frac{1}{\sqrt{k^2b^2 - j_{0s}^2}} + \sum_{s=S+1}^{\infty} \frac{j}{\sqrt{j_{0s}^2 - k^2b^2}} \right). \tag{4.73}$$

Here, in reality, the second summation cannot go to infinity because the expansion will break down as soon as $\alpha_s g \simeq 1$.

The zeroes of $Im\, D$ in Eq. (4.72) determine the peaks of resonances. If the summations are neglected, from Eq. (4.73), they occur at $k\Delta = \pi/2,\ 3\pi/2$, etc., which just correspond to resonances inside the corrugation or when the depth Δ is an odd number of the quarter wavelength. This contributes very sharp resonances. Usually only the first one will be visible because they are at very high frequencies. The first summation in D represents all the above-cutoff modes of waves that can propagate along the beam pipe so that the sharp resonances will be damped heavily. The second summation, which is imaginary, represents all the below-cutoff modes that attenuate along the beam pipe. Its effect can be thought of as fields clinging to the opening of the corrugation, thus making the corrugation depth Δ effectively longer and the resonance frequencies smaller. In fact, this is borne out mathematically, since this second summation is positive aside from the factor j while $\cot k\Delta$ is positive for $k\Delta$ smaller than $\pi/2$.

Figure 9 shows the plot of the impedance $Z_\parallel$ due to a corrugation of depth $\Delta/b = 0.1$ and half width $g/b = 0.025$. Equation (4.71) has been used; but the plots are exactly those given by Henke. We see a broad resonance with the resonant frequency shifted from $kb = \pi b/\Delta = 15.7$ to ~ 13. We also see notches located exactly at $kb = j_{0s}$, the zeroes of J_0 or the cutoff frequencies of the pipe. These notches are evident from Eq. (4.71), because when kb approaches j_{0S} only one term in the summation will contribute. Physically, since $2g \ll \lambda$, the wavelength, only the z-independent mode is favored in the region of the corrugation. At one of the cutoff frequencies, the mode that is just allowed is z-independent and is therefore favored and dominates over all others. This mode will not penetrate into the corrugation at all and, as a result, the beam does not see the corrugation at all. Or, this mode has a phase velocity that is infinite and will not interact with the particle beam which has a finite velocity; therefore $Z_\parallel$ vanishes. The plot also shows some sharp resonances just before the first few cutoff frequencies. According to Henke, they belong to well-trapped modes in the region of the cross section enlargement. The

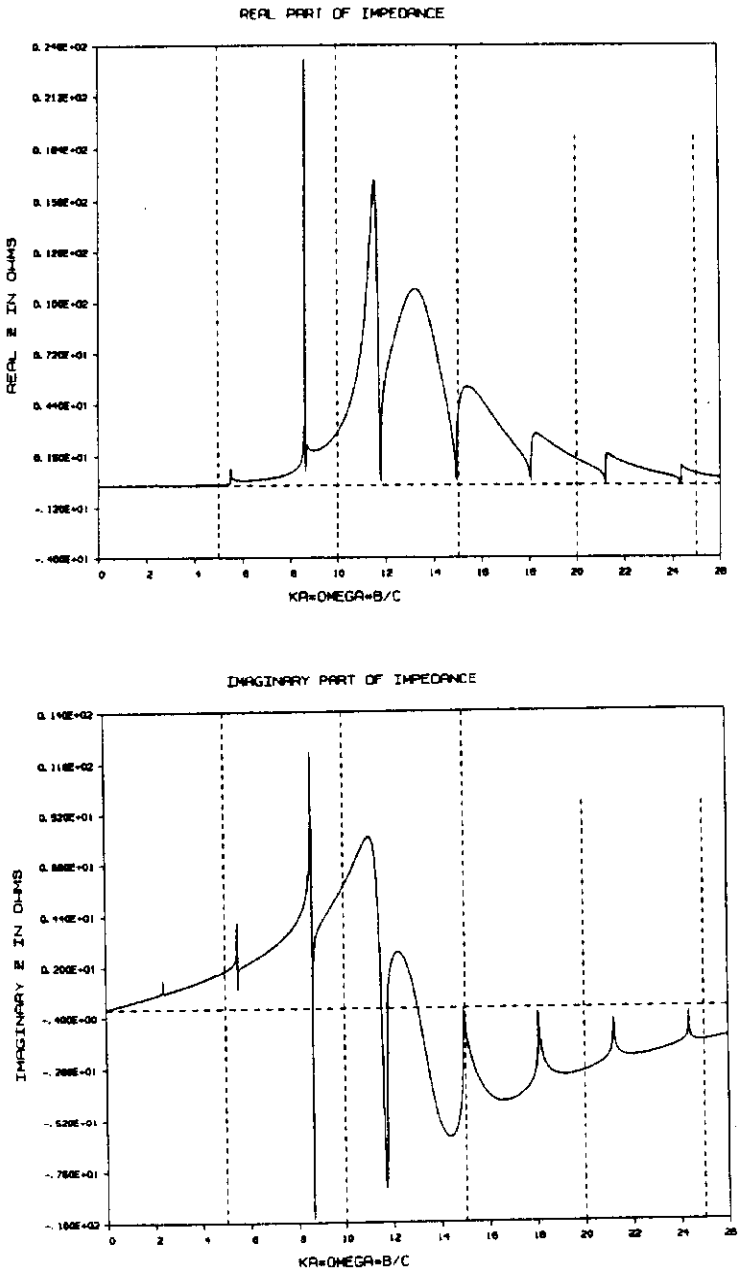

Figure 9: Real and imaginary parts of the longitudinal impedance of one corrugation of a bellows with half width $g/b = 0.025$ and depth $\Delta/b = 0.1$.

physical existence of such trapped modes is not clear at all. But mathematically it is clear. The admittance which is proportional to D has an imaginary part going to infinity at the zeroes of J_0. For frequencies below the first broad band, as it goes to infinity, it crosses the zero value twice, and, as a result, produces a sharp resonance there. For frequencies above the first broad band and far below the second, the imaginary part of the admittance is always positive; thus no sharp resonances are seen.

For a bellows with many corrugations, the total impedance is not just the sum of the impedances of the individual corrugations. This is because the corrugations are so close together that they interact with each other. However, the situation is not too bad. The notches tend to smooth out because the z-independent mode is no longer favored. But the overall broad band remains. However, there are other field structures too; they are mainly due to resonances across several corrugations. The position of the broad band and its Q-value are not altered much; they can therefore be estimated using Eq. (4.72) and possibly Eq. (4.73). The position and quality factor of the broad band k_0b are given approximately by

$$\begin{aligned} &Im\, D(k_0b) = 0, \\ &Q \sim \frac{kb}{2\,Re\, D}\frac{d\, Im\, D}{d(kb)}\bigg|_{kb=k_0b}. \end{aligned} \tag{4.74}$$

The solution of the first equation can only be found numerically. The peak impedance can be estimated by Eq. (4.72) by putting $kb = k_0b$. However, if k_0b is close to j_{0S}, the result should not be accurate.

For a bellows consisting of many corrugations, the standard procedure is to compute the wake function using the code[11] TBCI and obtain the impedance via a Fourier transform[13]. The code TBCI solves the Maxwell's equations in the time domain and calculate the wake function $\hat{W}(t)$ of a Gaussian bunch of unit charge and RMS length σ_ℓ,

$$\hat{W}(t) = \int d\tau q(\tau) W(t-\tau), \tag{4.75}$$

where W is the wake potential due to a point source discussed in the earlier sections and $q(\tau)$ the charge distribution of the bunch, which, in reality, is a truncated Gaussian (usually truncated at $\pm 5\sigma_\ell$). The Fourier transformation of Eq. (4.75) gives $\hat{Z}(\omega)$, the effective impedance seen by the bunch, and is related to the actual impedance seen by a point charge $Z(\omega)$ by

$$\hat{Z}(\omega) = Z(\omega) e^{-\frac{1}{2}(\omega\sigma_\ell/c)^2} \tag{4.76}$$

via Eq. (2.30) or Eq. (2.46). Knowing $\hat{Z}(\omega)$, the correct $Z(\omega)$ can be found.

In practice, $Z(\omega)$ can only be computed up to some limiting frequency due to the exponential factor in Eq. (4.76). For example, if we choose $\sigma_\ell = 3$ mm, the exponential factor drops to $\sim 5\%$ at $\omega/2\pi \sim 40$ GHz and not much information is retained. It appears that the best way to get to higher frequencies is to decrease the bunch length σ_ℓ. However, the mesh size has to be reduced at the same time. Too small a mesh size will increase the time of computation tremendously and will also exceed the limit of the code which allows for $\sim 60,000$ mesh points only. Too big a mesh size will also lead to error. As a rule of thumb, horizontally we need at least 4 to 5 mesh lines inside each corrugation of the bellows to get meaningful should be at least 4 to 5 times the mesh size.

We take as an example a bellows consisting of 15 rectangular corrugations with a depth of $\Delta = 4.875$ mm and period $p = 3$ mm. The beam pipe radius is $b = 1.65$ cm. The longitudinal and transverse wake functions are displaced in Fig. 10. The real and imaginary parts of $Z_\parallel$ are displaced in Fig. 10. The real and imaginary parts of $Z_\parallel$ are shown in Fig. 11. The transverse counterparts are displaced in Fig. 12. We see that both $Z_\parallel$ and $Z_\perp$ show a broad resonance near ~ 11.5 GHz and a smaller second resonance near ~ 37 GHz. The solution of Eq. (4.74) yields ~ 13 GHz for the first resonance with $Q \sim 6.6$. The actual resonant peak obtained by TBCI is much lower than this. Qualitatively, this may be due to the fact that, with many corrugations, the fields clinging to the opening of the corrugations extend farther into the beam pipe than the situation of only one corrugation. The second resonance is roughly three times away, agreeing with the approximate solutions of $\cot k_0\Delta = \pi/2$ and $3\pi/2$ for the first two resonances. Since the SSC RMS bunch length is 7 cm, the bunch spectrum will not extend to the second resonance. So we concentrate only on the first.

We see that the notches disappear. The other structures may be a result of the resonances of several corrugations as a whole and some are definitely computation noises. The small undulations are due to the truncation of the wake potentials. The peak impedances are roughly $Z_\parallel \sim 19\ \Omega$ and $Z_\perp \sim 610\ \Omega/\text{m}$ for *each* corrugation. When a charged particle passes through the corrugations, electromagnetic fields are left behind and trapped inside the corrugations. The high-frequency fields are resonances that are damped heavily if above cutoff, since the fields leak out. These give rise to one of the broad bands discussed above. At low frequencies, only magnetic flux can be trapped as depicted in Fig. 13(a), because the electric field cannot satisfy the required boundary conditions.

Due to a current $I(t) = I_0 e^{j\omega t}$, the magnetic flux trapped inside a corrugation or cavity of length ℓ is

$$\phi_t = \frac{\mu_0 I_0 \ell}{2\pi} \ln \frac{b+\Delta}{b}. \tag{4.77}$$

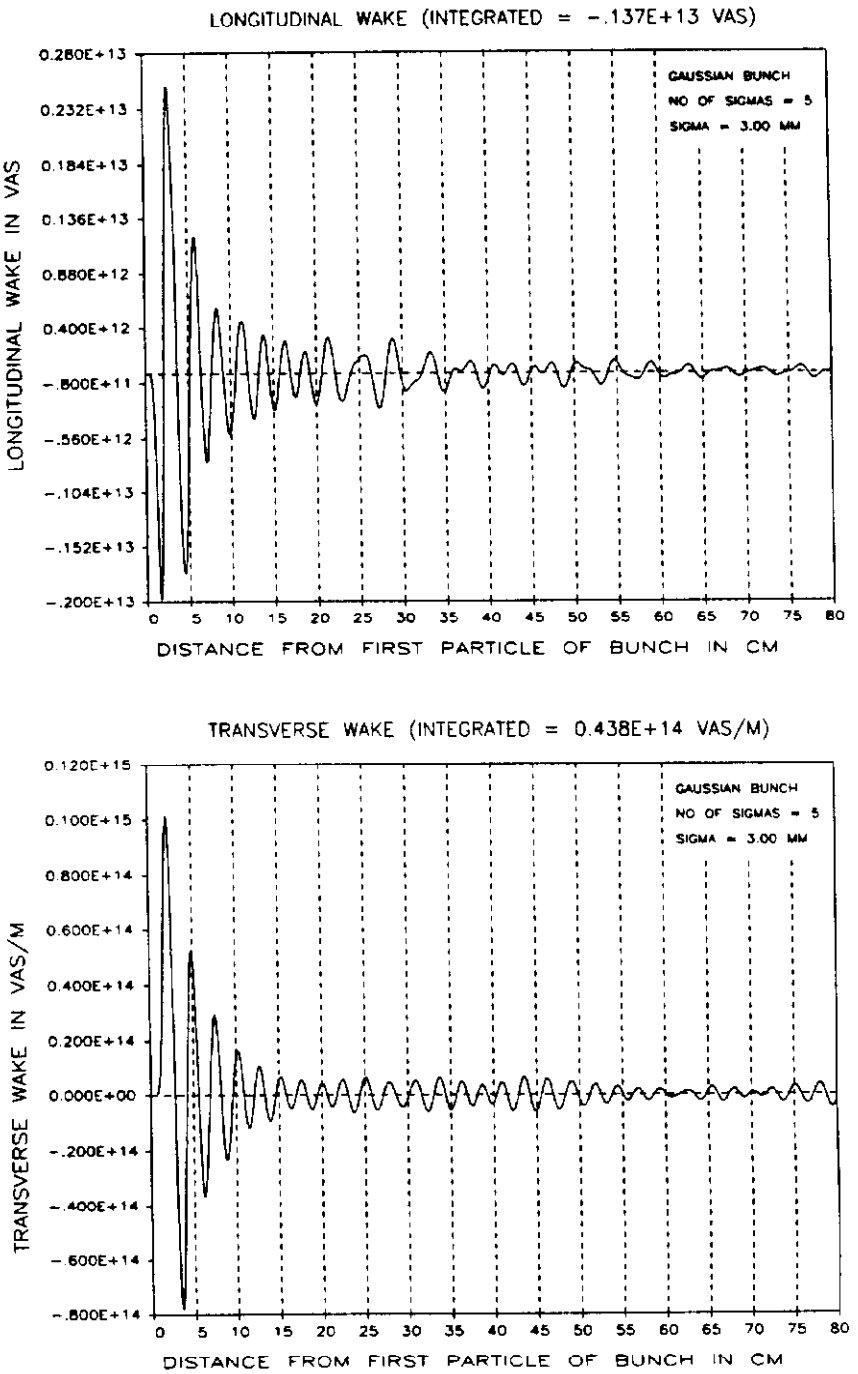

Figure 10: Longitudinal and transverse wake functions of 15 corrugations of a bellows with period 3 mm, depth 4.875 mm and beam pipe radius 1.65 cm.

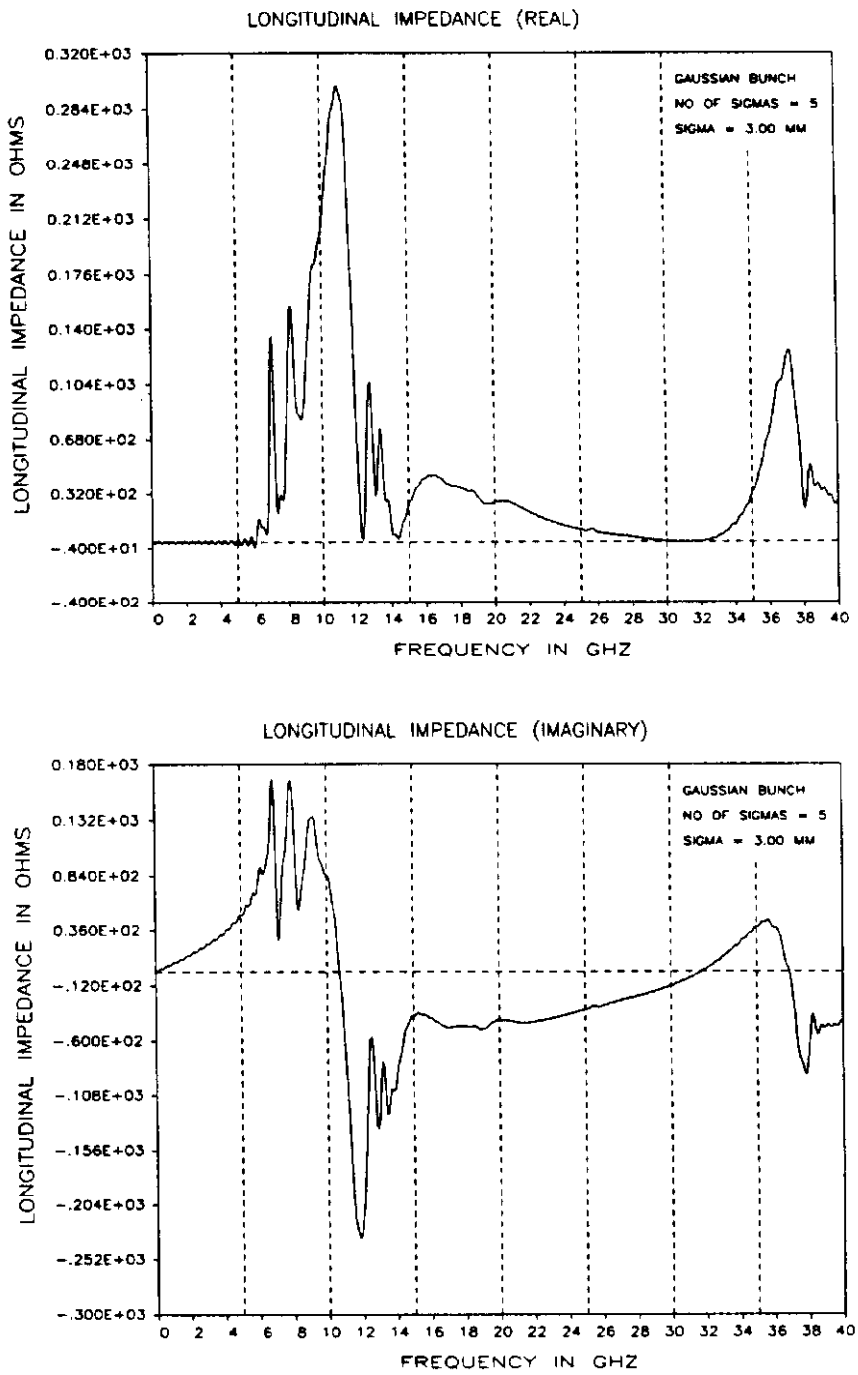

Figure 11: Longitudinal impedance of 15 corrugations of a bellows with period 3 mm, depth 4.875 mm and beam pipe radius 1.65 cm.

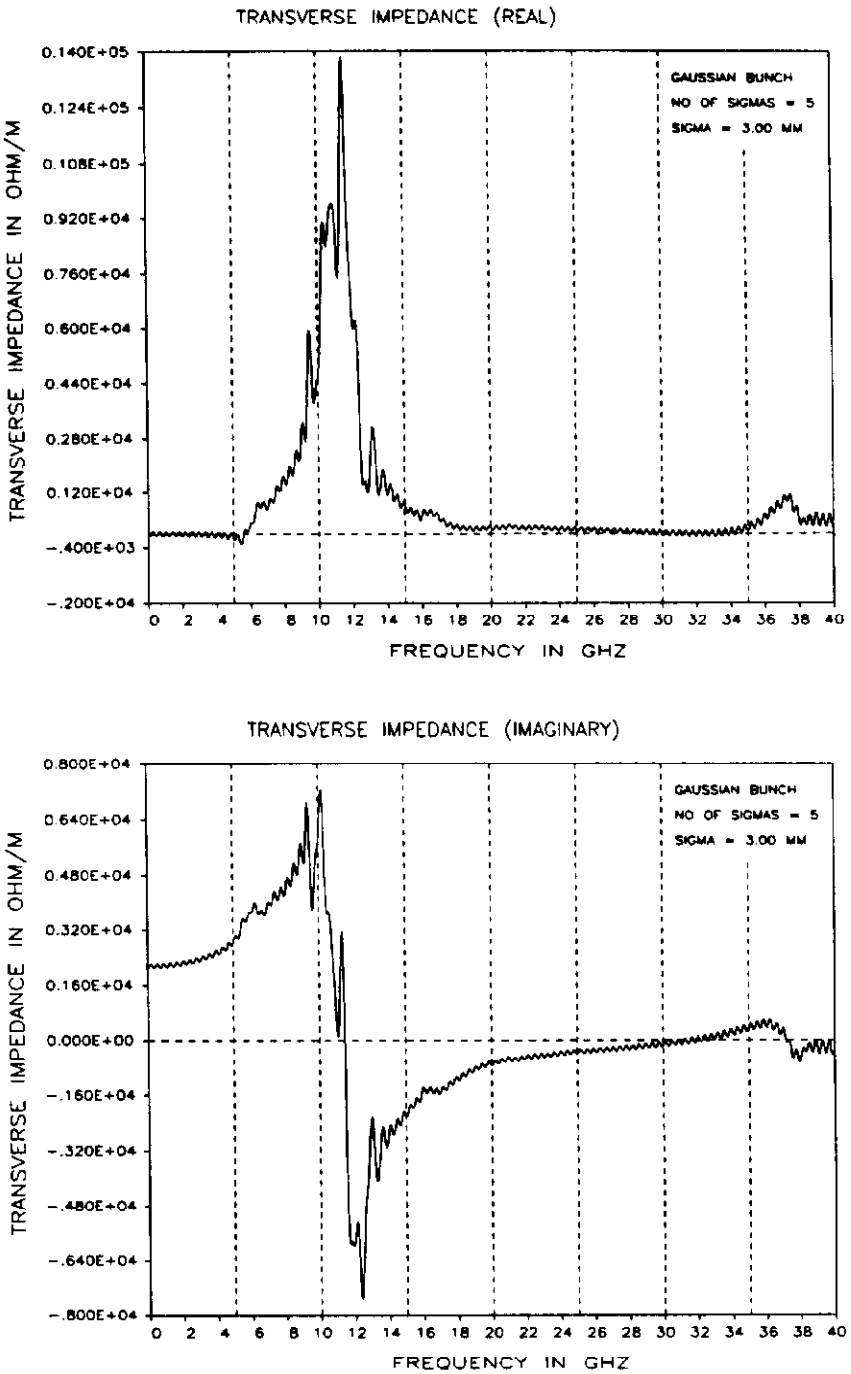

Figure 12: Transverse impedance of 15 corrugations of a bellows with period 3 mm, depth 4.875 mm and beam pipe radius 1.65 cm.

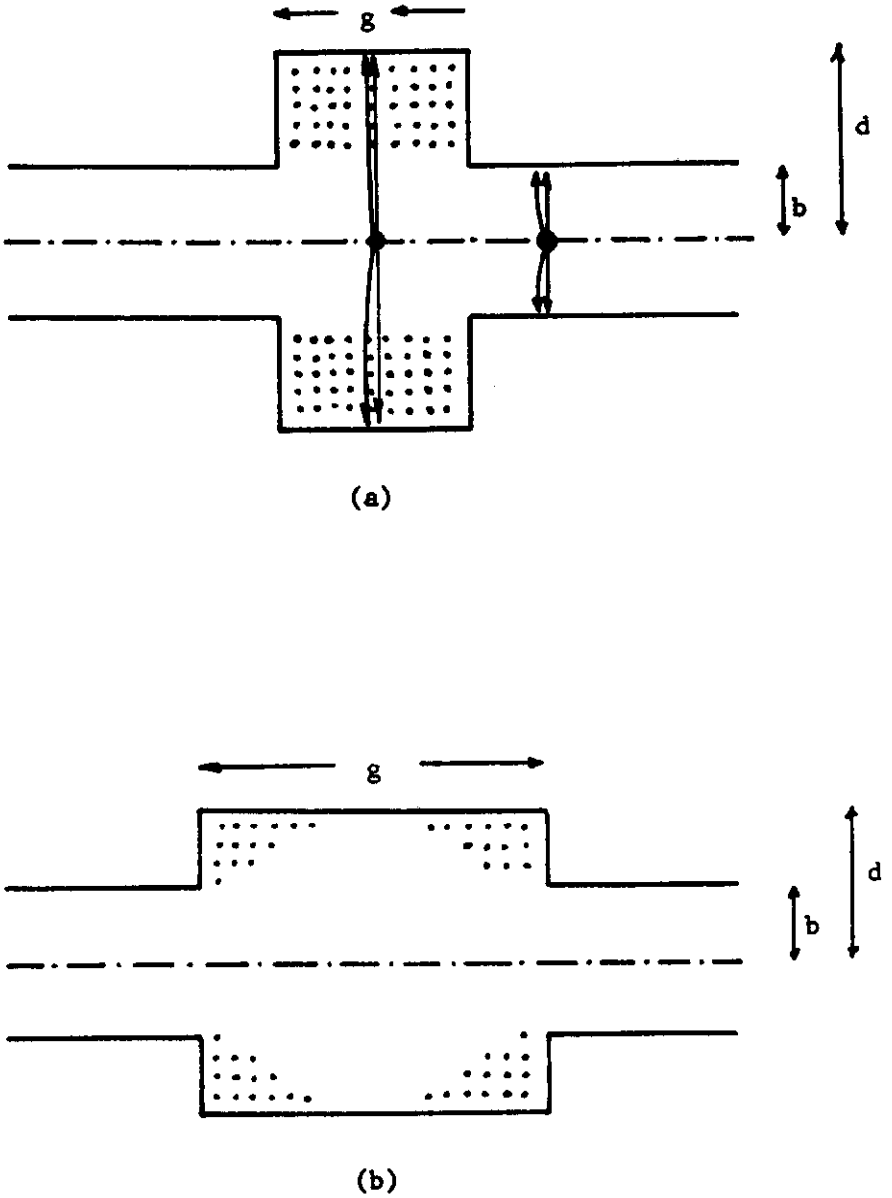

Figure 13: (a) At low frequencies, only magnetic flux (dots) can be trapped inside a cavity after the passage of a charged particle whose electric field lines are shown as solid arrows. (b) When the cavity width is much bigger than the step, only the magnetic flux near the corners can be trapped; the flux in the middle leaks away.

Only the flux between b and $b+\Delta$ has been included because the rest has been taken care of as space-charge contribution. The back e.m.f. induced on the beam is

$$\int E_z dz = -j\omega\phi_t. \tag{4.78}$$

Therefore, the longitudinal impedance per harmonic seen by the beam at low frequencies is[14]

$$\frac{Z_\parallel}{n} = j\frac{Z_0\beta\ell}{2\pi R}\ln\frac{b+\Delta}{b}, \tag{4.79}$$

where $Z_0 = 377\ \Omega$, R the ring radius and βc the beam particle velocity.

For the dipole mode, we can make use of the space-charge contribution in Eq. (4.15). The contribution of the magnetic field trapped is equal to the difference of the magnetic part of the space-charge impedance with pipe radius $b+\Delta$ and that with pipe radius b, i.e.,

$$Z_\perp = j\frac{Z_0\ell}{2\pi}\left[\frac{1}{b^2} - \frac{1}{(b+\Delta)^2}\right], \tag{4.80}$$

which can be rewritten as

$$Z_\perp = j\frac{Z_0\ell}{\pi b^2}\frac{S^2-1}{2S^2}, \tag{4.81}$$

where $S = (b+\Delta)/b$. A solution of the Maxwell's equations in the frequency domain[15] gives a result that alters the denominator from $2S^2$ to S^2+1. The difference is not big if $\Delta/b \ll 1$. Also in this limit, we find $Z_\perp \propto \Delta/b^3$ while $Z_\parallel \propto \Delta/b$.

Note that formulae (4.79) and (4.81) are good only when the length of the corrugation or cavity is less than the steps or $\ell \ll 2\Delta$. When $\ell \gg 2\Delta$ for a long cavity, only the flux near the corners will be trapped and that in the middle will leak away as depicted in Fig. 13(b). In that case, ℓ should be replaced by $\sim 2\Delta$ in the formulae.

Coming back to the bellows, formulae (4.79) and (4.81) give for *each* corrugation, $Z_\parallel/n = j1.77\times10^{-6}\ \Omega$ and $Z_\perp = j133\ \Omega/\text{m}$. From the TBCI computations, we can read off from Figs. 10 and 11 that $Z_\parallel/n = j1.81\times10^{-6}\ \Omega$ and $Z_\perp = j142\ \Omega/\text{m}$ per corrugation, which do not differ from our theoretical estimations by very much.

For 1.20 km of bellows with period $p = 3$ mm, there will be 400,000 corrugations. Therefore, they contribute at low frequencies $(Z_\parallel/n)_{\omega\to0} = j0.72\ \Omega$ and $(Z_\perp)_{\omega\to0} = j57\ \text{M}\Omega/\text{m}$. At the peak of the broad band around ~ 10.8 GHz, $(Z_\parallel/n)_{broad} = 2.5\ \Omega$ and $(Z_\perp)_{broad} = 240\ \text{M}\Omega/\text{m}$.

If only the broad band is retained for either the longitudinal and transverse impedances, the above analysis shows that the main features of the broad band can be estimated without the actual running of the time-consuming numerical codes[12].

The transverse impedance is too high or at least dangerous to transverse microwave instability and transverse mode-coupling instability. So the bellows corrugations must be shielded[13]. A typical shielded bellows package using sliding contact is sketched in Fig. 14(a). A gap is left between the two cylindrical shields to allow for the possible mechanical sliding. Its width has been exaggerated at $\Delta = 2$ mm. Each bellows package is assumed capable of absorbing a length of contraction of 8 cm during cool down. There are 5000 such bellows packages in the entire ring, with a maximum contraction of 400 m.

The impedances are again calculated by TBCI with Fourier transformations. For this example, we choose a gap g of 10 cm, a depth d of 5.5 mm, $p = 30$ cm so that the length of the whole package is 50 cm. The inner radius of the beam pipe is taken as 1.5 cm. In order to reduce the number of mesh points required, the actual calculations are done with the gap closed at A because any fields reflected from A will only affect a particle that is 60 cm behind the bunch head. The SSC bunch has a RMS length of only 7 cm. Thus, this approximation is good so far as single-bunch effects are concerned.

The results are shown in Fig. 14(b) and (c). The gap between the two cylindrical shieldings resembles an infinite coaxial transmission through which electromagnetic energy can leak away. The line has inner and outer radii 1.7 and 1.9 mm, or a characteristic impedance is $(377\ \Omega/2\pi)\ln(1.9/1.7) = 6.7\ \Omega$, in agreement with Fig. 14(b). This impedance will contribute to parasitic beam energy loss. If the end A is not closed, fields will be reflected back and forth with resonances at frequencies $0.5, 1.0, 1.5, \ldots$ GHz. However, such a complicated picture also produces the same single bunch effects[16].

The transmission line picture also allows a dipole TM mode or 'ring mode' with the azimuthal wavelength just equal to the circumference of the gap, or a frequency of $c/2\pi r = 2.8$ GHz, where $r \sim 1.8$ cm. Such a resonance is actually seen in Fig. 14(c).

The gap of length g between the point B and the end of the bellows package can be viewed as a wide and shallow cavity. Using the formula in Eq. (4.79) with the length ℓ replaced by 2×4 mm, we obtain at low frequencies, $Z_\parallel/n = j8.6 \times 10^{-6}\ \Omega$ in agreement with the initial slope of $Im\, Z_\parallel$ in Fig. 14(b). The transverse impedance obtained similarly from Eq. (4.81) is $Z_\perp = j990\ \Omega/\text{m}$ while Fig. 14(c) gives j1300 Ω/m. The discrepancy may be a result of the rough substitution of $\ell \sim 8$ mm. It may also be due to the influence of the resonance at 2.8 GHz.

For 5000 bellows packages, at low frequencies, $Z_\perp = j6.5\ \text{M}\Omega/\text{m}$ which is an order of magnitude less than that of the exposed bare corrugations. The longitudinal impedance at low frequencies is $Z_\parallel = 3.4\ \text{k}\Omega$ which can pose a threat to parasitic

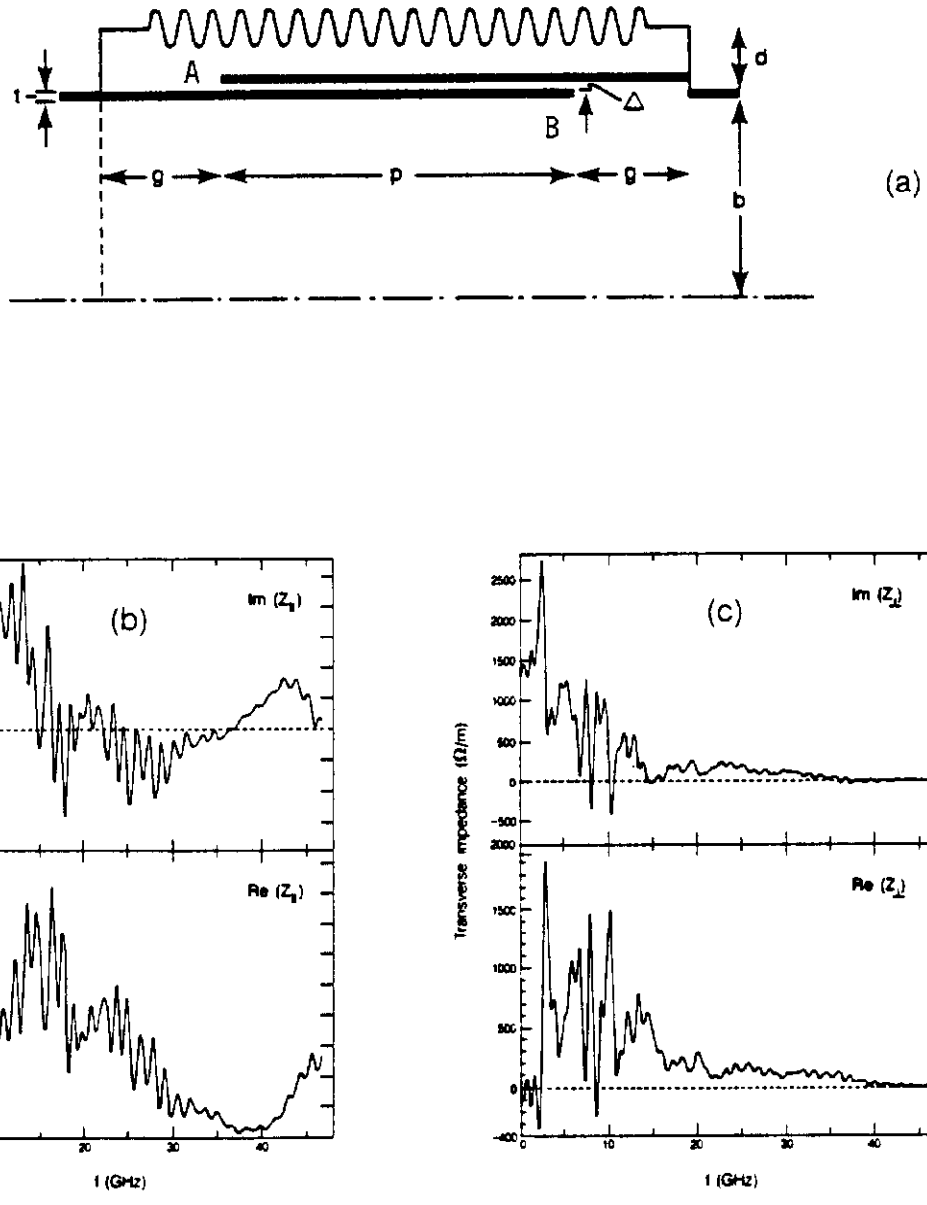

Figure 14: (a) A bellows package with sliding contact shielding in the expanded position. (b) Longitudinal and (c) transverse impedances per bellows package, parameters used being $b = 1.5$ cm, $g = 10$ cm, $p = 30$ cm, $t = 2$ mm, $\Delta = 2$ mm.

heating. However, this impedance is directly proportional to the sliding gap Δ which can actually be reduced. But only a reduction to $\Delta < 0.1$ mm will satisfy the allowable parasitic loss for the SSC. Another way is to put fingers at the entrance of the gap so that most of the energy leakage can be blocked. As a result, $Z_{\parallel}$ will be reduced drastically.

Recently, there is another code written by Gluckstern and Neri[17] to compute the longitudinal and transverse impedance of an obstacle of general shape above cutoff of the beam pipe. The final result can be given as an integral of the fields over the surface of the cavity or beam pipe surface only where the two are different. The fields and coupling impedances are then obtained using an adaptation of the code SUPERFISH[18]. Since the computation is done in the frequency domain, there is not any problem of noises due to the truncation of the wake potential and Fourier transform. The results show very clean plots of the impedances. However, tremendous computer time is required because the calculations are done at each individual frequency point.

Kickers

A kicker is a device to deflect a beam in the transverse direction in a short period of time. A simple-minded kicker is just a magnet. There are essentially two types of magnets: the window magnet in Fig. 15(a) and the C-type magnet in Fig. 15(b). The magnetic flux goes through the windings and returns through the core. The part that passes through the core does not link the coil windings and is therefore independent of the generator impedance or any load in the magnet circuit. However, the time variation of the flux does contribute to an inductive impedance to the beam. Also, the losses in the core due to the permeability hysteresis loop and eddy currents in the magnet laminations will contribute a real impedance. These contributions depend on the actual structure of the magnet core and the properties of its material, and are therefore not so easy to compute. The other part of the flux that links the core windings interacts directly with the beam. This effect can easily be estimated and we will derive it first[6].

Let us firstly study a window-frame magnet with height, width and length of the magnet interior equal to $2a$, $2b$ and ℓ. The magnet core, or the ferrite, is assumed to be perfect, or there is no loss due to eddy current and the magnetic permeability is infinite. Consider a beam current $I(t) = I_0 e^{j\omega t}$ passing through it but deviating horizontally from the central axis by an amount x_0. The magnetic field H that returns through the core on both sides will be exactly zero. If the magnet windings

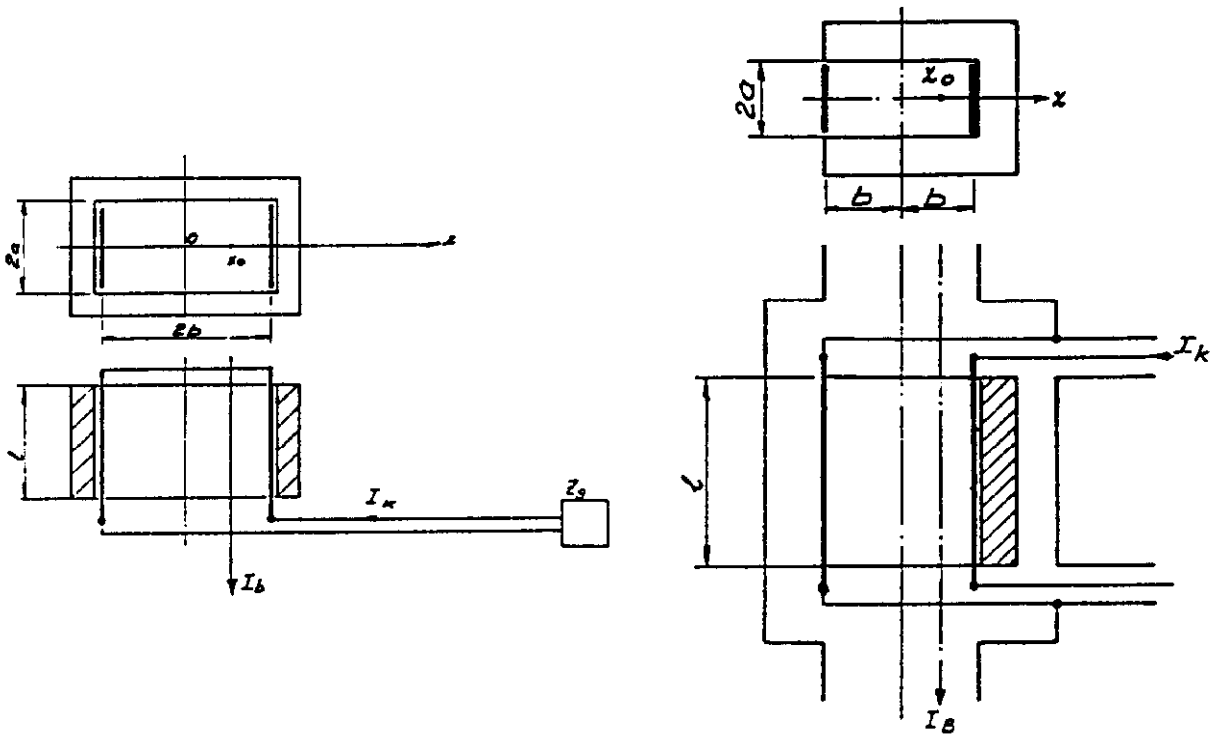

(a) (b)

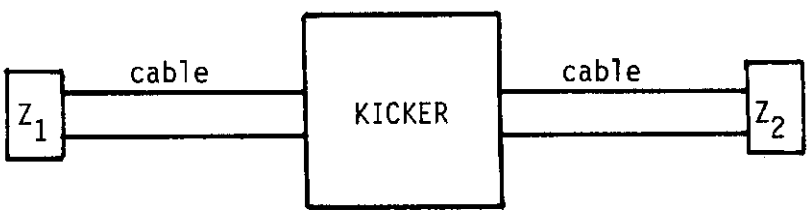

(c)

Figure 15: (a) Window-frame magnet and (b) C-type magnet viewed from front (upper figure) and top (lower figure). (c) Magnet circuit of a travelling-wave kicker.

of the single turn design carries a current I_k, the flux linking the beam is

$$\phi = \frac{\mu_0 I_k \ell x_0}{2a}, \tag{4.82}$$

where we have assumed that the permeability of the magnetic core is extremely large so that the magnetic field H is zero there. The mutual inductance from windings to beam is therefore

$$M(x_0) = \frac{\mu_0 \ell x_0}{2a}, \tag{4.83}$$

which is also equal to the mutual inductance from beam to windings. Thus, the particle beam will induce a voltage

$$V_k = j\omega M(x_0) I_0 \tag{4.84}$$

and a current $I_k = V_k/Z_k$ in the windings, where the impedance of the magnetic circuit is

$$Z_k = j\omega L + Z_g. \tag{4.85}$$

In above, Z_g is the generator and cable impedance while $L = \mu_0 b\ell/a$ the inductance of the windings. This current I_k in turn induces at the horizontal location x an e.m.f.

$$V = -j\omega M(x) I_k = \frac{\omega^2 M(x) M(x_0) I_0}{Z_k}. \tag{4.86}$$

According to Eq. (4.65), the *differential impedance* of Nassibian and Sacherer is

$$Z_\parallel(x, x_0) = \frac{\omega^2 M(x) M(x_0)}{Z_k}. \tag{4.87}$$

With $x \to x_0$, we get the longitudinal impedance at x_0,

$$Z_\parallel = \frac{\omega^2 \mu_0^2 \ell^2 x_0^2}{4a^2 Z_k}, \tag{4.88}$$

and, by differentiating with respect to x and x_0 according to Eq. (4.68), we get the horizontal transverse impedance

$$Z_\perp = \frac{c\omega \mu_0^2 \ell^2}{4a^2 Z_k}. \tag{4.89}$$

The situation of the C-magnet is similar. Here, the return magnetic flux passes through the core on one side of the windings only. Assuming a constant gap height of $2a$, the mutual inductance between windings and beam becomes

$$M(x_0) = \frac{x_0 + b}{2a} \mu_0 \ell, \tag{4.90}$$

and the impedances become

$$Z_{\parallel} = \frac{\omega^2 \mu_0^2 \ell^2 (x_0 + b)^2}{4a^2 Z_k}, \tag{4.91}$$

and

$$Z_{\perp} = \frac{c\omega \mu_0^2 \ell^2}{4a^2 Z_k}. \tag{4.92}$$

Note that, for the window-type magnet, the longitudinal impedance is proportional to the square of the beam deviation and is zero if the beam is at the center of the magnet.

When a kicker is fired, we would like the rise time and fall time to be fast so that only a particular bunch will be kicked leaving the others untouched. Therefore, we would like the voltage or current pulse that is fired into the kicker and the e.m.f. induced back in the windings to go one way and disappear instead of reflecting or ringing back and forth for a certain length of time. One method is to distribute capacitance between the windings so that the magnetic circuit appears as a transmission line with the same characteristic impedance Z_s as the cables attached to the ends of the windings. Such a kicker circuit is shown in Fig. 15(c), in which Z_1 and Z_2 are the impedance loads at the end of the cables including the generator. Usually, Z_1 and Z_2 are chosen to be Z_s also so that any voltage fired and the back e.m.f. induced will travel down the cables and will be totally absorbed without any reflection. Such a system is called a travelling-wave kicker[19].

Because capacitance C' is added across the windings so as to produce a characteristic impedance of Z_s, the phase velocity $v = 1/\sqrt{L'C'}$ of this section of transmission line of the windings will in general be much less than c. Here, L' and C' are the inductance and capacitance per unit length. Using $L' = \mu_0 b/a$, $Z_s = \sqrt{L'/C'}$, and $Z_0 = \mu_0 c = 377\ \Omega$, this velocity is given by

$$\frac{v}{c} = \frac{Z_s}{Z_0}\frac{a}{b}. \tag{4.93}$$

As an example, consider the SSC injection kicker which has a characteristic impedance of $Z_s = 16.6\ \Omega$, width $2b = 7.2$ cm, and height $2a = 4.5$ cm, the phase velocity $v/c = 0.028$. Thus, the transit time effect of the signal in the magnetic circuit must not be neglected.

The e.m.f. induced by the particle beam $I(t) = I_0 e^{j\omega t}$, which is x_0 away from the central axis, in the magnet winding element between s and $s + ds$ is

$$E e^{j\omega t} ds = j\omega I_0 e^{j\omega t} M(x_0) ds, \tag{4.94}$$

where the mutual inductance $M(x_0)$ is given by either Eq. (4.83) for a window-type magnet or Eq. (4.90) for a C-type magnet. The distance s is measured from the center of the winding so that $-\ell/2 \leq s \leq \ell/2$. The voltage at a point s_0 is due to one half the e.m.f. induced at earlier time to the left of s_0 and travelling with velocity v towards s_0 minus one half the e.m.f. induced at earlier time to the right and travelling with velocity towards s_0. In other words,

$$V(s_0) = \frac{E}{2} e^{j\omega t} \left[\int_{-\ell/2}^{s_0} e^{-jk(s_0-s)} ds - \int_{s_0}^{\ell/2} e^{-jk(s-s_0)} ds \right], \tag{4.95}$$

where

$$k = \frac{\omega}{v} = \frac{\omega \mu_0 b}{Z_s a} = \frac{\omega Z_0 b}{c Z_s a}, \tag{4.96}$$

and the transit time of the beam, which travels with velocity $\sim c$, through the kicker has been neglected. The integrations give the voltage distribution along the winding,

$$V(s_0) = \frac{E}{k} e^{j(\omega t - k\ell/2)} \sin k s_0. \tag{4.97}$$

Similarly, the current distribution along the winding is

$$I(s_0) = \frac{E}{2Z_s} e^{j\omega t} \left[\int_{-\ell/2}^{s_0} e^{-jk(s_0-s)} ds + \int_{s_0}^{\ell/2} e^{-jk(s-s_0)} ds \right], \tag{4.98}$$

or

$$I(s_0) = \frac{E}{jk} (1 - e^{-jk\ell/2} \cos k s_0). \tag{4.99}$$

Now, we can compute the impedances of the kicker. The power dissipated by the two termination loads is

$$P = \frac{1}{2Z_s} [|V(\ell/2|^2 + |V(-\ell/2)|^2], \tag{4.100}$$

which is equal to $\frac{1}{2} \mathcal{R}e\, Z_{\|} |I|^2$, or

$$\mathcal{R}e\, Z_{\|} = \frac{\omega^2 (b + x_0)^2 \mu_0^2 \ell^2}{8a^2 Z_s} \left(\frac{\sin \theta/2}{\theta/2} \right)^2, \tag{4.101}$$

where the mutual inductance $M(x_0)$ for a C-type magnet has been substituted. For a window magnet, Eq. (4.83) should be used. Note that this expression is the same as Eq. (4.91) derived above with the magnetic circuit impedance $Z_k = 2Z_s$ and multiplied by a transit factor, in which $\theta = k\ell = \omega\ell/v$ denotes the electrical length of the kicker winding. Putting $x_0 = 0$ for convenience and using Eq. (4.96),

considerable simplification can be obtained and the real part of the impedance becomes

$$\mathcal{R}e\, Z_{\parallel} = \frac{1}{2} Z_s \sin^2 \frac{k\ell}{2}. \tag{4.102}$$

The reactive part of the longitudinal impedance can be derived by computing the energy stored,

$$W_{mag} - W_{elect} = \frac{1}{2} \int_{-\ell/2}^{\ell/2} [L' |I(s)|^2 - C' |V(s)|^2] ds, \tag{4.103}$$

and equating the result to $\frac{1}{2} L_k |I_0|^2$, where L_k is the apparent inductance seen by the beam current I_0. Using Eqs. (4.94), (4.97), (4.99) and the fact that $C' = L'/Z_s^2$, we obtain

$$L_k = \frac{1}{4} L' \ell \left(1 - \frac{\sin k\ell}{k\ell} \right), \tag{4.104}$$

and

$$\mathit{Im}\, Z_{\parallel} = \frac{1}{4} Z_s (k\ell - \sin k\ell). \tag{4.105}$$

We want to point out that the $\mathcal{R}e\, Z_{\parallel}$ in Eq. (4.102) and $\mathit{Im}\, Z_{\parallel}$ in Eq. (4.105) do not satisfy Hilbert transformation. In fact, their frequency dependency resembles that for the stripline monitor. If we assume $\mathcal{R}e\, Z_{\parallel}$ to be correct, Hilbert transform will give an $\mathit{Im}\, Z_{\parallel}$ exactly the same as Eq. (4.105) but with a plus sign in front of $\sin k\ell$ instead. The reason is not clear at the moment. The same comment applies to $Z_{\perp}$ in Eqs. (4.107) and (4.108) in below.

Now the factor

$$\left(\frac{b + x_0}{b} \right) \left(\frac{b + x}{b} \right) \tag{4.106}$$

can be placed back in Eqs. (4.102) and (4.105) to obtained the *differential impedance* $Z_{\parallel}(x, x_0)$. Then, by differentiating with respect to x and x_0 according to Eq. (4.68), we obtain immediately

$$\mathcal{R}e\, Z_{\perp} = \frac{Z_0 \ell}{4ab} \frac{1}{k\ell} (1 - \cos k\ell), \tag{4.107}$$

$$\mathit{Im}\, Z_{\perp} = \frac{Z_0 \ell}{4ab} \left(1 - \frac{\sin k\ell}{k\ell} \right). \tag{4.108}$$

Equation (4.107) is also the same as Eq. (4.92) with Z_k replaced by $2Z_s$ and the transit factor multiplied.

Now we try to take into account the fact that the ferrite is not perfect. Let B_g and B_f be the magnetic flux intensities in the magnet gap and the ferrite core

respectively. For the window-magnet, using Ampere law around one of the plate current I_k, we get

$$\frac{B_g}{\mu_0}2a + \frac{B_f}{\mu_0\mu_f}(2a+2b) = I_k, \tag{4.109}$$

where μ_f is the relative magnetic permeability of the ferrite which is no longer assumed to be infinite. The path length through the ferrite core has been assumed to be $\sim (2a+2b)$, where $2a$ and $2b$ are respectively the width and height of the magnet. The amount of magnetic flux for a length ℓ of magnet in the magnet gap is

$$\phi_t = 2b\ell B_g, \tag{4.110}$$

which is also given by

$$\phi_t = 2s\ell B_f, \tag{4.111}$$

since only half of the flux will go around one side of the magnet core and the flux will penetrate only a skin depth s of the ferrite. Combining Eqs. (4.109)-(4.111), we obtain[20]

$$\phi_t = \frac{I_k e^{-a/s}}{R_A + \frac{1}{2}R_F}, \tag{4.112}$$

where

$$R_A = \frac{a}{\mu_0 b\ell} \tag{4.113}$$

is the reluctance of the magnet gap,

$$R_F = \frac{2(a+b)}{\mu_f\mu_0 s\ell} \tag{4.114}$$

is the reluctance of one half of the frame, and the factor $e^{-a/s}$ is added to take care of the loss due to eddy current. The skin depth can be derived easily in the usual way but with both the conductive and displacement currents included. We obtain

$$\frac{1}{s} = Im\left[\mu_0\mu_f\left(\omega^2\epsilon_0\epsilon_f - j\omega\sigma\right)\right]^{1/2},$$

or

$$s = \frac{c}{\omega}\left(\frac{2}{\epsilon_f\mu_f}\right)^{1/2}\left\{\left[1+\left(\frac{c^2\mu_0\sigma}{\omega\epsilon_f}\right)^2\right]^{1/2} - 1\right\}^{-1/2}, \tag{4.115}$$

where σ is the conductivity, μ_f the relative magnetic permeability, and ϵ_f the relative electric permittivity of the ferrite.

As a result, the flux linking a displaced beam in Eq. (4.82) should be replaced by

$$\phi = \frac{x_0}{2b} \frac{I_k e^{-a/s}}{R_A + \frac{1}{2} R_F}. \tag{4.116}$$

Again, the factor of $\frac{1}{2}$ in front of R_F in Eq. (4.116) comes about because only one half of the magnetic flux in the magnet gap returns through one side of the window frame. For a C-type magnet, this factor is not present. Thus, we have taken into account the finite reluctance of the frame and the penetration depth of the magnetic field in the magnetic material or, more explicitly, the fact that the finite resistivity acts as a screen, by means of eddy currents, against the magnetic field. The net result is the multiplication of the impedances in Eqs. (4.102), (4.105), (4.107) and (4.108) by the factor

$$F = \left(\frac{e^{-a/s}}{1 + R_F/2R_A} \right)^2. \tag{4.117}$$

For the SSC, there are 10 injection kickers and 8 abort kickers. Their specifications are listed in Table 1. The longitudinal and transverse impedances of the 10

	Injection Kicker	Abort Kickers
Type	C-magnet	Window-frame
Number of modules	10	8
Length of each module, ℓ	0.8 m	1.375 m
Core	Ferrite	Tape wound
Half height, a	22.5 mm	20 mm
Half width, b	36 mm	37.5 mm

Table 1: Specifications of the SSC injection and abort kickers

injection and 8 abort kickers have been calculated by Colton and Wang[21]. They took the circumference of the SSC ring as 82.9 km and the characteristic impedance of the kickers as $Z_s = 25\ \Omega$. They took, for the ferrite, the relative permeability $\mu_f = 100$, the relative permittivity $\epsilon_f = 11$, and the resistivity $\sigma = 10^{-3}$ mho/m. For abort kickers, the loss factor F in Eq. (4.117) was assumed to be unity and the beam offset was taken as $x_0/b = 0.1$. Their results are displayed in Fig. 16.

rf Cavities

The rf cavities are large cavities along the beam pipe so that the fundamental mode provides an accelerating field at the designed frequency. There are a number of higher parasitic modes of high Q's up to the cutoff frequency of the connecting

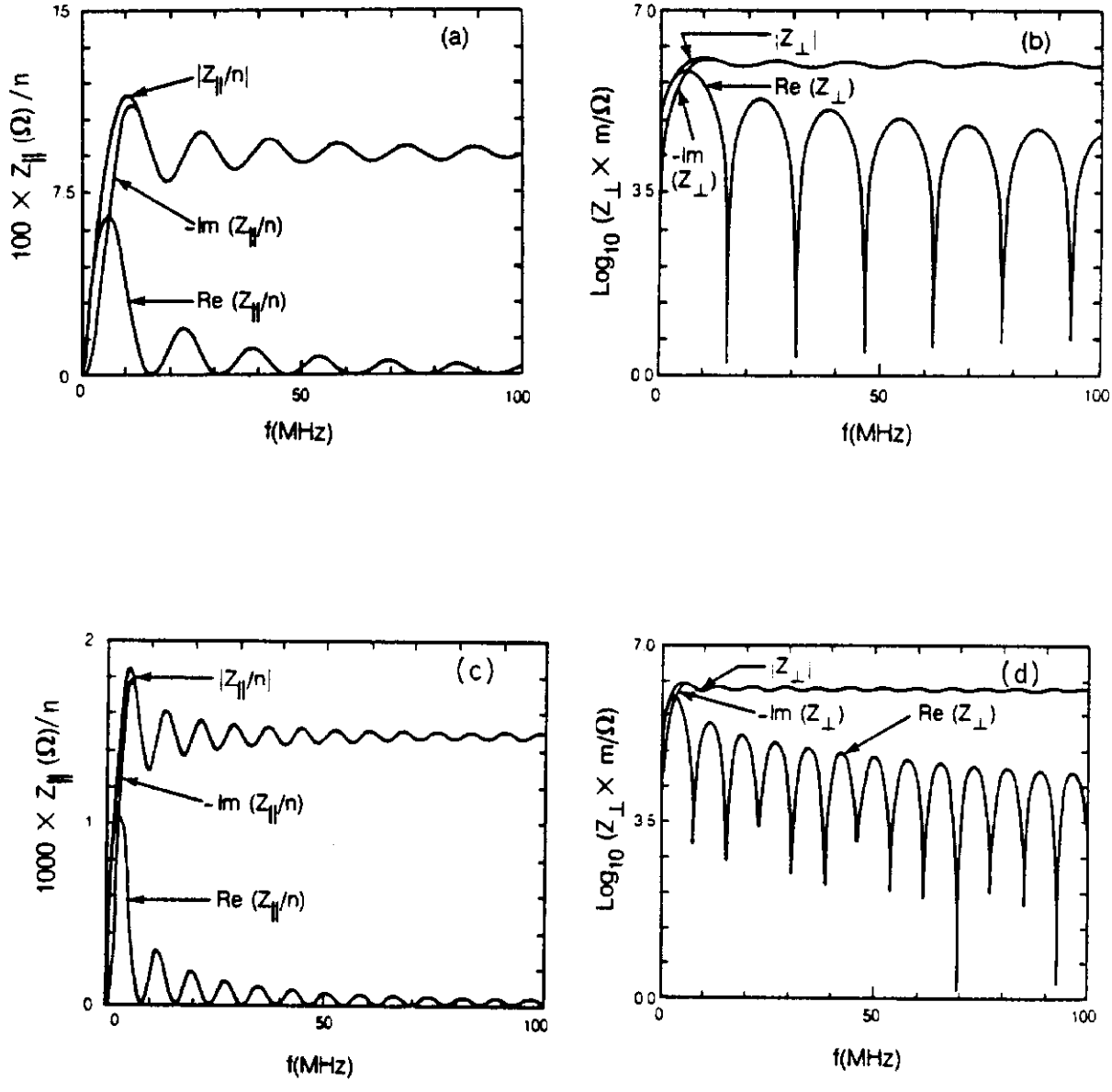

Figure 16: (a) Longitudinal and (b) transverse impedances of the injection kickers. (c) Longitudinal and (d) transverse impedances of the abort kickers.

sidepipe. After that, the resonances become broadened due to the fact that fields can now travel along the beam pipe. The narrow resonances below cutoff correspond to wake fields that ring in the cavity for a large number of rf oscillations, causing a bunch to interact with other bunches, and, if the beam intensity is large enough, leading to coupled bunch-instabilities.

The SSC rf cavities have not been definitely designed yet. In Fig. 17, we show a rf cavity in the PEP storage ring at SLAC. Because of the large radius compared

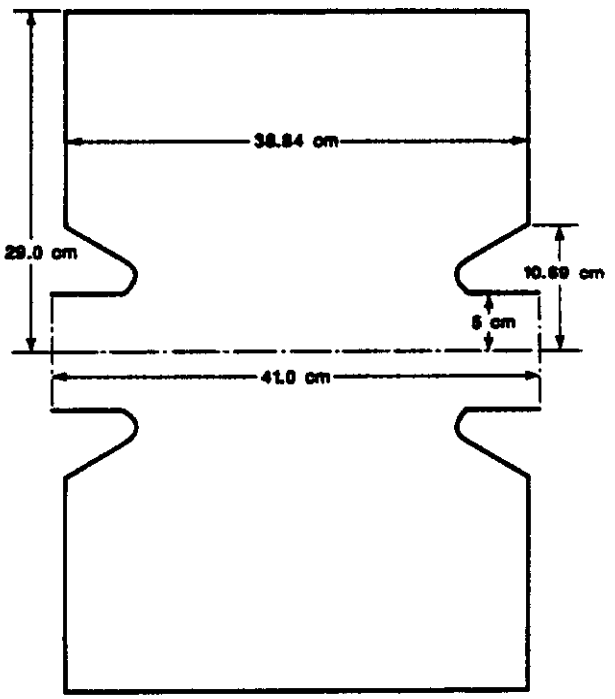

Figure 17: Plain view and dimensions of the cylindrical PEP rf cavity cell with fundamental accelerating frequency 358.8 MHz.

with that of the sidepipe, as an estimate, we can assume the ends of the cavity as closed. Then, accurate up the cutoff, the cavity approximately a pill-box cylindrical cavity which has been studied in detail[22]. For the m-th multipole of a cavity of radius d and length ℓ, the resonance frequencies of the TM modes are given by

$$\frac{\omega_{mnp}}{c} = \left(\frac{x_{mn}^2}{d^2} + \frac{p^2\pi^2}{\ell^2} \right)^{1/2}, \tag{4.118}$$

and those of the TE modes by

$$\frac{\omega_{mnp}}{c} = \left(\frac{x_{mn}'^2}{d^2} + \frac{p^2\pi^2}{\ell^2} \right)^{1/2}, \tag{4.119}$$

where x_{mn} and x'_{mn} are the n-th zero of the Bessel function of order m, J_m, and that of the J'_m respectively. The electric fields and magnetic fields are also given in the book by Jackson[22] so that the quality factors and shunt impedances can also be estimated.

A numerical calculation can be done for a cavity of irregular shape using the code URMEL written by Weiland[23]. It assumes the cavity to be closed and solves the Maxwell's equations with boundary conditions as an eigenvalue equation in the frequency domain. Its results list the frequency, Q, shunt impedance R_s and R_s/Q for each mode assuming a very high conductivity of the cavity walls. It can also plot the electric and magnetic fields for each mode so that we know which mode we are looking at. This code also has a version for a cavity that is not cylindrically symmetric. Recently, Weiland is modifying the code so that it can take up the problem of *open* sidepipes also.

Conclusion

Inside the vacuum chamber, there are also other types of discontinuities, for examples, Lambertson magnets, port holes for vacuum pumps, beam collimators, septa, etc. Also, the issue of synchrotron radiation is important here because of the high energies of today's machines. Some of them have been treated in detail elsewhere while some have not yet been computed with satisfaction. Because of the limitation of time and space, they are not reviewed here.

References

[1] A. W. Chao, in *Second Summer School on High Energy Particle Accelerators*, Stanford Linear Accelerator Center, Stanford, August 1982, ed. M. Month.

[2] W. K. H. Panofsky and W. A. Wenzel, Rev. Sci. Instrum. **27**, 967 (1956).

[3] J. D. Jackson, SSC Central Design Group Internal Report No. SSC-N-110 (1986).

[4] K. Y. Ng, in *Accelerator Physics Issues for a Superconducting Super Collider*, Ann Arbor, December 1983, ed. M. Tigner, University of Michigan Report No. UM HE 84-1.

[5] R. Shafer, in *Report of the SSC Impedance Workshop*, Lawrence Berkeley Laboratory, Berkeley, June 1985, ed. J. Bisognano, SSC Central Design Group Internal Report No. SSC-SR-1017.

[6] G. Nassibian and F. Sacherer, Nucl. Instr. and Meth. **159**, 21 (1979).

[7] In *Superconducting Super Collider Conceptual Design*, ed. J. D. Jackson, September 1986, SSC Internal Report No. SSC-SR-2020, Section 5.12.2.

[8] M. Tigner, SSC Central Design Group Internal Report No. SSC-N-136.

[9] H. Henke, CERN Report CERN-LEP-RF/85-41.

[10] R. L. Gluckstern, private communication.

[11] T. Weiland, DESY Report 82-015 (1982) and Nucl. Instr. and Meth. **212**, 13 (1983).

[12] K. Y. Ng, Fermilab Report FN-449; K. Y. Ng, Proceedings of the 1987 Particle Accelerator Conference, Washington, D.C., March 1987.

[13] K. Bane and R. Ruth, in *Report of the SSC Impedance Workshop*, Lawrence Berkeley Laboratory, Berkeley, June 1985, ed. J. Bisognano, SSC Central Design Group Internal Report No. SSC-SR-1017; J. Bisognano and K. Y. Ng, ibid.; K. Y. Ng, ibid.

[14] E. Keil and W. Zotter, Particle Accelerators **3**, 11 (1972).

[15] K. Y. Ng, Fermilab Report FN-389.

[16] K. Y. Ng, in *Proceedings of the 1986 Summer Study on the Physics of the Superconducting Super Collider*, Snowmass, Colorado, June 1986.

[17] R. L. Gluckstern and F. Neri, IEEE Trans. Nucl. Sc. **5**, 2403 (1985).

[18] K. Halbach and R. F. Holsinger, Particle Accelerators **7**, 213 (1976).

[19] G. Nassibian CERN Reports CERN/PS 84-25 (BR) (1984) and CERN 85-68 (BR) (1986).

[20] G. Shaffer, V. G. Vaccaro, and G. Wüstefeld, KFA Julich Internal Report 2.5.GS/VV/GW.1 (1981).

[21] E. Colton and T. S. Wang, SSC Central Design Group Internal Report No. SSC-N-144.

[22] J. D. Jackson, *Classical Electrodynamics*, 2nd edition, John Wiley & Sons.

[23] C. Palm, U. Van Rienen and T. Weiland, DESY Report No. M-85-11 (1985).